Incorporating Interventional Independence Improves Robustness against Interventional Distribution Shift

Anonymous authors
Paper under double-blind review

Abstract

We consider learning discriminative representations of variables related to each other via a causal graph. To learn representations that are robust against interventional distribution shifts, the training dataset is augmented with interventional data in addition to existing observational data. However, even when the underlying causal model is known, existing approaches treat interventional data like observational data, ignoring the independence relations resulting from these interventions. This leads to representations that exhibit large disparities in predictive performance on observational and interventional data. The performance disparity worsens when the quantity of interventional data available for training is limited. In this paper, (1) we first identify a strong correlation between this performance disparity and adherence of the representations to the statistical independence conditions induced by the underlying causal model during interventions. (2) For linear models, we derive sufficient conditions on the proportion of interventional data during training, for which enforcing statistical independence between representations corresponding to the intervened node and its non-descendants during interventions can lower the test-time error on interventional data. Following these insights, we propose RepLIn, an algorithm to explicitly enforce this statistical independence during interventions. We demonstrate the utility of RepLIn on synthetic and real face image datasets. Our experiments show that RepLIn is scalable with the number of nodes in the causal graph and is suitable to improve the robustness of representations against interventional distribution shifts of both continuous and discrete latent variables compared to the ERM baselines.

1 Introduction

We consider the problem of learning discriminative representations corresponding to latent random variables from their observable data. The relationship between these latent variables can be modeled using directed acyclic graphs (DAGs) called *causal graphs*. These latent variables usually correspond to semantic concepts such as the color of an object, the level of glucose in the blood, and a person's age. Causal modeling allows manually altering the causal graph and observing its effects on the data, for instance, by consuming an insulin inhibitor and measuring the glucose level in the blood. This procedure is known as a *causal intervention*, and the data collected through this procedure is called *interventional data*. In contrast, data collected without intervention is known as *observational data*. Several types of interventions are possible on a causal graph, of which we are interested in *hard interventions* where we manually set the value of one or more variables. Intervening on a node renders it statistically independent of its *parent nodes* in the causal graph[1]. See (Peters et al., 2017, Chapter 6) and (Pearl, 2009, Chapter 3).

Suppose the latent variables are A and B, such that $A \to B$ (A *causes* B) during observations. An attribute-specific representation $\boldsymbol{F}_A$ corresponding to A learned by a model from observational training data alone may contain information about its child node B due to the association between A and B. Subsequently, these models show a performance drop on data collected through intervention on B during inference. In

[1]For ease of use, we refer to "statistical independence" as "independence", and "hard interventions" as "interventions". We will also use "features" to describe the representations a model learns from data.

other words, these models are not robust against *interventional distribution shifts*. Interventional data samples are included in the training data to learn models that are robust to interventional distribution shifts. For example, in (Sauer & Geiger, 2021; Gao et al., 2023), interventional data was generated using data augmentations to train image classification models that were invariant to texture and background. In some works such as (Arjovsky et al., 2019; Heinze-Deml & Meinshausen, 2021), interventional data is treated merely as data sourced from different domains or *environments*, and they do not consider the *explicit* statistical independence relations that arise from interventions. As we demonstrate, ignoring these independence relations may result in representations that are still susceptible to interventional distribution shifts during inference. Additionally, performing interventions is often challenging, thus limiting the amount of interventional data available for training. Therefore, causally motivated learning is necessary to improve the robustness of learned representations against interventional distribution shifts.

We first consider a simple case study in which we observe that models that do not learn independent representations during interventions show a performance drop on interventional data. We then derive sufficient conditions on the proportion of interventional data during training, for which enforcing linear independence between interventional features of linear models during training can reduce test-time error on interventional data. Following the theoretical assessment, we propose "Representation Learning from Interventional Data" (**RepLIn**), an algorithm to train models with improved robustness against interventional distribution shifts. We confirm the utility of RepLIn on synthetic (Sec. 5.1) and real face image datasets (Sec. 5.2) and demonstrate its scalability to the number of nodes (Sec. 6.2).

To summarize our contributions,

- We demonstrate a positive correlation between accuracy drop during interventional distribution shift and dependence between representations corresponding to the label node and its children. We refer to this as "interventional feature dependence" (Sec. 3.3).
- We theoretically explain why linear ERM models are susceptible to interventional distribution shifts in the regime of linear causal models. In the same setting, we theoretically and empirically show that enforcing linear independence between interventional features improves robustness when sufficient interventional data is available during training and establish the sufficient condition (Sec. 3.4).
- We propose a novel training algorithm that combines these insights and demonstrates that this model minimizes the drop in accuracy under interventional distribution shifts by explicitly enforcing independence between interventional features (Sec. 4).

2 Related Work

Identifiable Causal Representation Learning (ICRL) (Locatello et al., 2019; Schölkopf et al., 2021; Hyvärinen et al., 2024) seeks to learn representations of the underlying causal model under certain assumptions (Hyvärinen et al., 2024), and is, therefore, important to interpretable representation learning. However, we are interested in a broader class of discriminative representation learning when some underlying causal relations are known. In contrast to learning the entire causal model, we seek to exploit the known independence relations from interventions to learn discriminative representations that are robust against these interventions. We provide a detailed review of ICRL in App. C.

Interventional data is key in causal discovery (Eberhardt et al., 2005; Yu et al., 2019; Ke et al., 2019; Lippe et al., 2022a; Wang et al., 2022) as one can only retrieve causal relations up to Markov equivalent graph without interventions or assumptions on the causal model. For example, known interventional targets have been used for unsupervised causal discovery of linear causal models (Subramanian et al., 2022), interventional and observational data have been leveraged for training a supervised model for causal discovery (Ke et al., 2022), and interventions with unknown targets were used for differentiable causal discovery (Brouillard et al., 2020). Interventional data also find applications in reinforcement learning (Gasse et al., 2021; Ding et al., 2022) and recommendation systems (Zhang et al., 2021; Krauth et al., 2022; Luo et al., 2024). While this body of work focuses on discovering causal relations in the data, our work considers how to leverage known causal relations to learn data representations that are robust to distribution shifts induced by interventions.

Training with group-imbalanced data leads to models that suffer from group-bias during inference. In such cases, resampling the data according to the inverse sample frequency can improve generalization and robustness. Studies such as (Gulrajani & Lopez-Paz, 2021; Idrissi et al., 2022) have shown that ERM with resampling is effective against spurious correlations and is a strong baseline for domain generalization. Recent work such as dynamic importance reweighting (Fang et al., 2020), SRDO (Shen et al., 2020), and MAPLE (Zhou et al., 2022) *learn to resample* using a separate validation set that acts as a proxy for the test set. However, learning such a resampling requires a large dataset of both *observational* and *interventional* data, which is often not practically feasible. In contrast, we will exploit known independence relations during interventions to improve robustness to interventional distributional shifts.

3 The Learning from Interventional Data Problem

Notation: Random variables and random vectors are denoted by regular (e.g., A) and bold (e.g., $\boldsymbol{a}$) sans-serif uppercase characters, respectively. The distribution of a random variable A is denoted by P_A.

We now formally define the problem of interest in this paper, namely *learning discriminative representations that are robust against interventional distribution shifts*, in general terms, and examine a specific case study in Sec. 3.1. The learning problem is characterized by a DAG $\mathcal{G}$ that causally relates our attributes of interest $A_1, \ldots, A_m$, and B. Let $\mathbf{Pa}_B = \{A_1, \ldots, A_m\}$ denote the parents of the attribute B. These attributes along with other unobserved exogenous variables $\boldsymbol{U}$, generate the observable data $\boldsymbol{X}$, i.e., $\boldsymbol{X} = g_{\boldsymbol{X}}(B, A_1, \ldots, A_m, \boldsymbol{U})$. During interventions, the variable B is set to values drawn from a known distribution independent of $\mathbf{Pa}_B$. Therefore, the post-intervention variable B (denoted by $\tilde{B}$) is statistically independent of its parents, i.e., $\tilde{B} \perp\!\!\!\perp \mathbf{Pa}_B$, as shown in Fig. 1. Although $g_{\boldsymbol{X}}$ is not affected by this intervention, the distribution of $\boldsymbol{X}$ (now denoted by $\boldsymbol{X}'$) will change since it is a function of B. Note that to learn representations that are robust against distribution shift due to intervention on B, our setting does not provide the knowledge of any node apart from B and its parents in this causal graph or of any causal relations between $A_1, \ldots, A_m$. We also do not have restrictions on the functional form of causal relations between $A_1, \ldots, A_m, B$, and $\boldsymbol{X}$, or on their marginal distributions. For training, data samples from both observational and interventional distributions are available, i.e., $\mathcal{D}^{\text{train}} = \mathcal{D}^{\text{obs}} \cup \mathcal{D}^{\text{int}}$ where $\mathcal{D}^{\text{obs}} \sim P(\boldsymbol{X}, B, A_1, \ldots, A_m)$ and $\mathcal{D}^{\text{int}} \sim P(\boldsymbol{X}', \tilde{B}, A_1, \ldots, A_m)$. Given $\mathcal{D}^{\text{train}}$ and $\mathcal{G}$, the goal is to learn attribute-specific discriminative representations $\boldsymbol{F}_B = h_B(\boldsymbol{X})$ and $\boldsymbol{F}_{A_i} = h_{A_i}(\boldsymbol{X})$ that are robust against distribution shifts due to intervention on B.

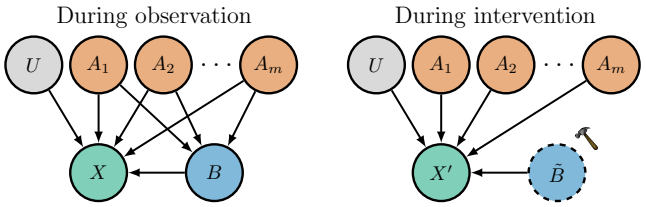

Figure 1: **Causal graph modification due to intervention:** During observation, B is the effect of its parent variables $\mathbf{Pa}_B = \{A_1, \ldots, A_m\}$. When we intervene on B, it becomes statistically independent of its parents.

3.1 Does Accuracy Drop during Interventions Correlate with Interventional Feature Dependence?

First, we consider a motivating case study on a synthetic dataset and establish a correlation between the accuracy drop on interventional data and statistical dependence between the attribute representations under intervention. We will then estimate the strength of this correlation and theoretically investigate whether this correlation can be exploited to improve the robustness against interventional distribution shifts.

Problem Setting: Consider the causal graph shown in Fig. 2a. Here, A and B are binary random variables that generate the observed data $\boldsymbol{X} \in \mathbb{R}^2$. $\boldsymbol{X}$ is also affected by an unobserved noise variable $\boldsymbol{U}$. Therefore, functionally $\boldsymbol{X} = g_{\boldsymbol{X}}(A, B, \boldsymbol{U})$. A itself could be a function of unobserved random factors that are of no predictive interest to us. Therefore, we model $A \sim \text{Bernoulli}(0.6)$. The distribution of B is only affected by A, as denoted by the arrow between them. Analytically, $B := A$, where $:=$ indicates the causal assignment operator, following (Peters et al., 2017). Visually, the observed data looks like a windmill. The value of A determines the windmill's blade, and B determines the radial distance. We shear the windmill blades according to a sinusoidal function of the radial distance. To make the data more stochastic, the points' precise angle and radial distance are sampled from an unobserved distribution independent of A and B. In

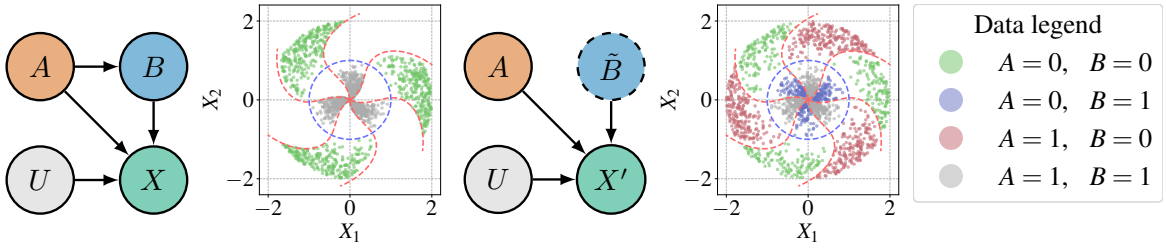

(a) Observational graph and data (b) Interventional graph and data

Figure 2: **An illustration of Windmill Dataset:** A and B are binary random variables that are causally linked to each other and $\boldsymbol{X}$, as shown in (a). By intervening on B as shown in (b), we make $A \perp\!\!\!\perp \tilde{B}$. $\boldsymbol{X} = g_{\boldsymbol{X}}(A, B, \boldsymbol{U})$ where $\boldsymbol{U}$ denotes unobserved noise variables. The true decision boundaries for predicting A and B from $\boldsymbol{X}$ are shown in red and blue dashed lines, respectively. See App. D for a detailed description.

Fig. 2b, we intervene on B, modeled as $\tilde{B} \sim \text{Bernoulli}(0.5)$. This induces a change in the distribution of B and subsequently that of $\boldsymbol{X}$. Since the intervention is independent of A, $\tilde{B}$ is also independent of A, denoted by removing the arrow between A and $\tilde{B}$. Note that $g_{\boldsymbol{X}}$ is unaffected by this intervention. The exact mathematical formulation of the data-generating process is provided in App. D.

Learning task: The task is to accurately predict A and B from $\boldsymbol{X}$ at test time. We have N samples for training, where βN are interventional and $(1-\beta)N$ are observational with $0 < \beta < 1$ typically being a small value. For this demonstration, we set $N = 40,000$, $\beta = 0.01$. Therefore, we have 39,600 observational and 400 interventional samples. We train a feed-forward network with two hidden layers to learn representations $\boldsymbol{F}_A$ and $\boldsymbol{F}_B$ corresponding to A and B, respectively. We normalize them by dividing each by their corresponding L_2 norm. Separate linear classifiers predict A and B from $\boldsymbol{F}_A$ and $\boldsymbol{F}_B$ respectively. By construction, $g_{\boldsymbol{X}}$ in the data-generating process is a one-to-one mapping. Therefore, predicting A and B from $\boldsymbol{X}$ accurately is possible. However, the true decision boundary for A is more complex than that of B[2]. Therefore, the model may rely on information from B to predict A due to their association during observation, similar to the concept of simplicity bias from (Shah et al., 2020). As a result, $\boldsymbol{F}_A$ may contain information about B even during interventions when $A \perp\!\!\!\perp B$.

ERM version	Accuracy in predicting A			Accuracy in predicting B			NHSIC
	Observation	Intervention	Relative drop	Observation	Intervention	Relative drop	
Vanilla	99.97	58.56	0.414	100	100	0	0.786
w/ Resampling	93.24	68.65	0.264	100	99.99	10^{-4}	0.537

Table 1: The relative drop in accuracy in predicting A correlates well with a gap in the measure of dependence between the learned representations on interventional data.

Observations: Following the standard ERM framework, the cross entropy errors in predicting A and B from $\boldsymbol{F}_A$ and $\boldsymbol{F}_B$, respectively, provide the training signal. The statistical loss function can be written as $\mathcal{L}_{\text{total}}(f, \boldsymbol{X}) = \mathbb{E}_{P_{\text{train}}}[\mathcal{L}_{\text{pred}}(f, \boldsymbol{X})]$. The training distribution is a mixture of observational and interventional distributions with $(1-\beta)$ and β acting as the corresponding mixture weights. Thus, $\mathcal{L}_{\text{total}}(f, \boldsymbol{X}) = (1-\beta)\mathbb{E}_{P_{\text{obs}}}\left[\mathcal{L}_{\text{pred}}(f, \boldsymbol{X}^{\text{obs}})\right] + \beta\mathbb{E}_{P_{\text{int}}}[\mathcal{L}_{\text{pred}}(f, \boldsymbol{X}^{\text{int}})]$. Tab. 1 shows the accuracy of ERM in predicting A and B on observational and interventional data during validation. Ideally, *we expect no drop in accuracy from observation to intervention* if the learned representations are robust against interventional distribution shift. However, we observe that ERM performs only slightly better than random chance in predicting A on interventional data. As a remedy, we consider a stronger version of ERM by sampling observational and interventional data in separate batches. This is equivalent to sampling interventional data $\left(\frac{1-\beta}{\beta}\right)$-times as observational data. Therefore, we refer to this version as "ERM-Resampled". The equivalent loss for a learning function f in ERM-Resampled is $\mathcal{L}_{\text{total}}(f, \boldsymbol{X}) = \mathbb{E}_{P_{\text{obs}}}\left[\mathcal{L}_{\text{pred}}(f, \boldsymbol{X}^{\text{obs}})\right] + \mathbb{E}_{P_{\text{int}}}[\mathcal{L}_{\text{pred}}(f, \boldsymbol{X}^{\text{int}})]$. Note

[2]We informally define "complexity" as the minimum polynomial degree required to approximate the decision boundary.

that β does not appear in $\mathcal{L}_{\text{total}}(f, \boldsymbol{X})$ due to resampling. Although ERM-Resampled performs better than vanilla ERM, we observe that ERM-Resampled still exhibits a large drop in predictive accuracy between observational and interventional data during inference.

3.2 Measuring Statistical Dependence Between Interventional Features

A key characteristic of hard interventions in causal graphs is that the variable being intervened upon becomes independent of all its nondescendants. Since the predictive accuracy on the parent node is affected by intervention, we hypothesize that *the representation corresponding to the parent node is dependent on the child node during intervention.* Therefore, to verify our hypothesis, we measure the dependence between the representations. We measure the dependence between the representations instead of between the representations and the latent attributes because we aim to learn robust representations for every attribute.

Dependence Measure: To measure dependence between a pair of high-dimensional continuous random variables $\boldsymbol{X}$ and $\boldsymbol{Y}$, we use HSIC (Gretton et al., 2005), a non-parametric measure of dependence. Given N i.i.d. samples $\mathcal{X} = \left\{\boldsymbol{x}^{(i)}\right\}_{i=1}^{N}$ and $\mathcal{Y} = \left\{\boldsymbol{y}^{(i)}\right\}_{i=1}^{N}$ from $\boldsymbol{X}$ and $\boldsymbol{Y}$, empirical HSIC between these samples can be computed as $\text{HSIC}(\mathcal{X}, \mathcal{Y}) = \frac{1}{(N-1)^2}\text{Trace}\left[\boldsymbol{K}_X \boldsymbol{H} \boldsymbol{K}_Y \boldsymbol{H}\right]$, where $\boldsymbol{H}$ is the $N \times N$ centering matrix, and $\boldsymbol{K}_X, \boldsymbol{K}_Y \in \mathbb{R}^{N \times N}$ are Gram matrices whose $(i,j)^{\text{th}}$ entries are $k_X\left(\boldsymbol{x}^{(i)}, \boldsymbol{x}^{(j)}\right)$ and $k_Y\left(\boldsymbol{y}^{(i)}, \boldsymbol{y}^{(j)}\right)$, respectively. Here, k_X and k_Y are the kernel functions associated with a universal kernel (e.g., RBF kernel). Since HSIC is unbounded, we normalize it as $\text{NHSIC}(\mathcal{X}, \mathcal{Y}) = \frac{\text{HSIC}(\mathcal{X},\mathcal{Y})}{\sqrt{\text{HSIC}(\mathcal{X},\mathcal{X})\,\text{HSIC}(\mathcal{Y},\mathcal{Y})}}$, following (Li et al., 2021).

We use the NHSIC metric to compare the statistical dependence between the features in the WINDMILL problem. Tab. 1 shows the difference in NHSIC values between the features F_A and F_B from interventional data. We observe that ERM-Resampled learns features with less statistical dependence during interventions than vanilla ERM. A larger interventional feature dependence indicates a larger violation of the underlying statistical independence relations that result from interventions in the causal graph.

3.3 Strength of Correlation between Drop in Accuracy and Interventional Features Dependence

How strong is the observed correlation between the dependence of features and the drop in accuracy? For a given combination of predictive task and dataset, does it hold for a variety of hyperparameter settings? To answer these questions, we train several models under the ERM-Resampled setting described in Sec. 3.1. To learn representations, we use feed-forward networks, each with one to six hidden layers and with 20 to 200 hidden units. We also randomly set the number of training epochs to use early-stopping as a regularizer, as described in (Sagawa et al., 2020). To measure the robustness of a model to interventional distribution shift, we evaluate the relative drop in accuracy between observational and interventional data: $\text{Rel.}\Delta = \frac{\text{Obs acc.} - \text{Int acc.}}{\text{Obs acc.}}$.

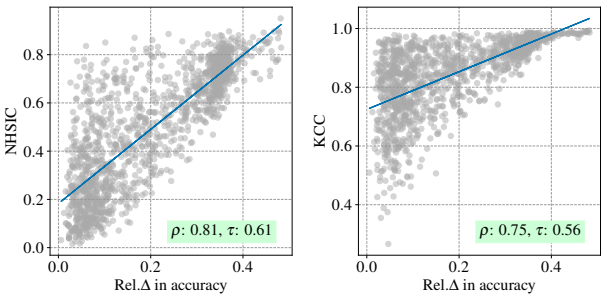

(a) Rel.Δ against NHSIC (b) Rel.Δ against KCC

Figure 3: Across models with different capacities, a relative drop in accuracy is always accompanied by interventional feature dependence, while the corollary does not hold. Interventional feature dependence is measured using NHSIC and KCC.

In Fig. 3, we plot the relative drop in accuracy against the interventional feature dependence. In addition to NHSIC, we also use kernel canonical correlation (KCC) (Bach & Jordan, 2002) to measure the dependence. From the plots, we infer that *a relative drop in accuracy is always accompanied by interventional feature dependence.* The strength of the correlation between the relative drop in accuracy and interventional feature dependence is quantitatively measured using Spearman rank correlation coefficient (ρ) (Spearman, 1904) and Kendall rank correlation coefficient (τ) (Kendall, 1938). In Fig. 3a, $\rho = 0.81$ and $\tau = 0.61$, indicating that the correlation we noted in Sec. 3.2 can be observed for a wide range of models. A similarly strong correlation can be observed between the relative drop in accuracy and KCC in Fig. 3b.

3.4 Will Minimizing Dependence between Interventional Features Improve Robustness?

Fig. 3 showed that strong interventional feature dependence always accompanies a large relative drop in accuracy. Based on this correlation, we may ask the following question: *will minimizing interventional feature dependence improve the robustness to interventional distribution shifts?* We consider a linear causal model to answer this question theoretically. The detailed proof of each step is provided in App. B.

Causal Model: We use the causal model shown in Fig. 2a with A and B being continuous random variables. A and B are causally related during observation as $B \coloneqq w_{AB}A$. The observed data signal $\boldsymbol{X}$ is generated from A and B as $\boldsymbol{X} \coloneqq \begin{bmatrix} X_A \\ X_B \end{bmatrix} + \boldsymbol{U}$, where $X_A \coloneqq w_A A$ and $X_B \coloneqq w_B B$. $\boldsymbol{U} \coloneqq \begin{bmatrix} U_A \\ U_B \end{bmatrix}$ is exogenous noise. U_A and U_B are independent of A and B respectively. We intervene on B as shown in Fig. 2b, severing the causal relation between A and B. The intervened variable is denoted as B' and $B' \perp\!\!\!\perp A$.

Learning model: Similar to the case study, the task is to predict the latent variables A and B from observed data signal $\boldsymbol{X}$. The training dataset is sampled from a training distribution P_{train} that contains observational and interventional samples. We model P_{train} as a mixture of observation distribution P_{obs} and interventional distribution P_{int} with $(1-\beta)$ and β acting as the mixture weights, i.e., $P_{\text{train}} = (1-\beta)P_{\text{obs}} + \beta P_{\text{int}}$. We use linear models to learn attribute-specific representations $\boldsymbol{F}_A$ and $\boldsymbol{F}_B$, from which predictions $\hat{A}$ and $\hat{B}$, respectively, are made using the classifiers. The linear models are parameterized by $\boldsymbol{\Theta}^{(A)}$ and $\boldsymbol{\Theta}^{(B)}$, and the classifiers are parameterized by $\boldsymbol{c}^{(\mathsf{A})}$ and $\boldsymbol{c}^{(\mathsf{B})}$.

Statistical Risk: The parameter matrix of the linear feature extractor described before can be written in terms of its constituent parameter vectors as $\boldsymbol{\Theta}^{(A)} = \begin{bmatrix} \boldsymbol{\theta}_A^{(A)\top} \\ \boldsymbol{\theta}_B^{(A)\top} \end{bmatrix}$. Assuming zero mean for all latent variables, the statistical squared error of an arbitrary model in predicting A from an interventional test sample $\boldsymbol{X}$ is,

$$E_A = \underbrace{\left(1 - w_A \boldsymbol{c}^{(\mathsf{A})\top}\boldsymbol{\theta}_A^{(A)}\right)^2 \rho_A^2 + \left(\boldsymbol{c}^{(\mathsf{A})\top}\boldsymbol{\theta}_A^{(A)}\right)^2 \rho_{\boldsymbol{U}_A}^2}_{E_A^{(1)}} + \underbrace{\left(w_B \boldsymbol{c}^{(\mathsf{A})\top}\boldsymbol{\theta}_B^{(A)}\right)^2 \rho_{B'}^2 + \left(\boldsymbol{c}^{(\mathsf{A})\top}\boldsymbol{\theta}_B^{(A)}\right)^2 \rho_{\boldsymbol{U}_B}^2}_{E_A^{(2)}} \tag{1}$$

where $\rho_A^2 = \mathbb{E}_{P_{\text{int}}}\left[A^2\right]$, $\rho_{B'}^2 = \mathbb{E}_{P_{\text{int}}}\left[B'^2\right]$, $\rho_{\boldsymbol{U}_A}^2 = \mathbb{E}_{P_{\text{int}}}\left[U_A^2\right]$, and $\rho_{\boldsymbol{U}_B}^2 = \mathbb{E}_{P_{\text{int}}}\left[U_B^2\right]$. The statistical risk can be split into two components: (1) $E_A^{(1)}$ in terms of A and U_A, and (2) $E_A^{(2)}$ in terms of B and U_B. $E_A^{(2)} \neq 0$ when $\boldsymbol{\theta}_B^{(A)} \neq \boldsymbol{0}$. A non-zero $\boldsymbol{\theta}_B^{(A)}$ indicates that $\boldsymbol{\phi}^{(\mathsf{A})}$ is a function of X_B, i.e., it learns a spurious correlation with B. Thus the prediction $\hat{A}$ is susceptible to interventions on B. In contrast, a robust model will have $\boldsymbol{\theta}_B^{(A)} = \boldsymbol{0}$, and thus $E_A^{(2)} = 0$. Derivation of Eq. (1) is provided in App. B.1.

Optimal ERM model: The optimal ERM model can be obtained by minimizing the expected risk in predicting the latent attributes. Since parameters are not shared between the prediction of $\boldsymbol{a}$ and $\boldsymbol{b}$, we can consider their optimization separately. We will consider the optimization of parameters for predicting $\boldsymbol{a}$ since we are interested in the performance drop in predicting A from interventional data.

$$\boldsymbol{\Theta}^{(A)*}, \boldsymbol{c}^{(\mathsf{A})*} = \underset{\boldsymbol{\Theta}^{(A)}, \boldsymbol{c}^{(\mathsf{A})}}{\operatorname{argmin}} \mathbb{E}_{P_{\text{train}}}\left[\left(A - \boldsymbol{c}^{(\mathsf{A})\top}\boldsymbol{\Theta}^{(A)\top}\boldsymbol{X}\right)^2\right] \tag{2}$$

For a given training error, there is no unique solution for $\boldsymbol{\Theta}^{(A)}$ and $\boldsymbol{c}^{(\mathsf{A})}$. Therefore, we can equivalently optimize for $\boldsymbol{\psi}_A = \boldsymbol{c}^{(\mathsf{A})\top}\boldsymbol{\Theta}^{(A)\top}$. We can write $\boldsymbol{\psi}_A = \begin{bmatrix} \psi_1 \\ \psi_2 \end{bmatrix}$ where $\psi_1 = \boldsymbol{c}^{(\mathsf{A})\top}\boldsymbol{\theta}_A^{(A)}$ and $\psi_2 = \boldsymbol{c}^{(\mathsf{A})\top}\boldsymbol{\theta}_B^{(A)}$.. The learning objective in Eq. (2) then reduces to,

$$\boldsymbol{\psi}_A^* = \underset{\boldsymbol{\psi}_A}{\operatorname{argmin}}\, \mathbb{E}_{P_{\text{train}}}\left[\left(A - \boldsymbol{\psi}_A \boldsymbol{X}\right)^2\right] \tag{3}$$

We can solve Eq. (3) by setting the gradients to zero. To check the robustness of the optimal ERM model, we can verify whether $\psi_2^* = 0$ or not since a robust model will have $\boldsymbol{\theta}_B^{(A)} = \boldsymbol{0}$. Solving Eq. (3), we get:

$$\psi_2^* = \frac{-(1-\beta) w_B w_{AB} \sigma_A^2 \sigma_{U_A}^2}{T} \neq 0$$

where T is a non-zero scalar. This implies that $E_A^{(2)} \neq 0$ in optimal ERM models. *Therefore, optimal ERM are not robust against interventional distribution shift.* The detailed derivation is provided in App. B.2.

Minimizing linear dependence: In Sec. 3.3, we showed that dependence between interventional features correlated positively with the drop in accuracy on interventional data. We will now verify if minimizing dependence between interventional features can minimize the drop in accuracy. The interventional features are given by $\boldsymbol{F}_A = \boldsymbol{\Theta}^{(A)\top}\boldsymbol{X}$ and $\boldsymbol{F}'_B = \boldsymbol{\Theta}^{(B)\top}\boldsymbol{X}$.

$$\boldsymbol{F}_A = \boldsymbol{\Theta}^{(A)\top}\boldsymbol{X} = X_A\boldsymbol{\theta}_A^{(A)} + X_B\boldsymbol{\theta}_B^{(A)}$$
$$\boldsymbol{F}'_B = \boldsymbol{\Theta}^{(B)\top}\boldsymbol{X} = X_A\boldsymbol{\theta}_A^{(B)} + X_B\boldsymbol{\theta}_B^{(B)}$$

For ease of exposition, we will minimize the linear dependence between interventional features instead of enforcing the full statistical independence we described in Sec. 3.2. Following the definition of HSIC (Gretton et al., 2005), the linear dependence in interventional features can be defined as follows[3],

$$\text{Dep}\left(\boldsymbol{F}_A, \boldsymbol{F}'_B\right) = \left\|\mathbb{E}_{P_{\text{int}}}\left[\boldsymbol{F}_A\boldsymbol{F}_B'^{\top}\right]\right\|_F^2 \tag{4}$$

Leveraging the independence relations during interventions, we can expand Eq. (4) as,

$$\left\|\mathbb{E}_{P_{\text{int}}}\left[\boldsymbol{F}_A\boldsymbol{F}_B'^{\top}\right]\right\|_F^2 = \left\|(w_A^2\rho_A^2 + \rho_{\boldsymbol{U}_A}^2)\boldsymbol{\theta}_A^{(A)}\boldsymbol{\theta}_A^{(B)\top} + (w_B^2\rho_{B'}^2 + \rho_{\boldsymbol{U}_B}^2)\boldsymbol{\theta}_B^{(A)}\boldsymbol{\theta}_B^{(B)\top}\right\|_F^2 \tag{5}$$

The dependence loss is thus the Frobenius norm of a sum of rank-one matrices. There are three classes of solutions that minimize Eq. (5): (1) $\boldsymbol{\theta}_A^{(A)} = \boldsymbol{\theta}_B^{(A)} = \boldsymbol{\theta}_A^{(B)} = \boldsymbol{\theta}_B^{(B)} = \mathbf{0}$, (2) $\boldsymbol{\theta}_A^{(A)} = \pm\gamma\boldsymbol{\theta}_B^{(A)}$ and $\gamma\boldsymbol{\theta}_A^{(B)} = \mp\boldsymbol{\theta}_B^{(B)}$ for some scalar $\gamma \neq 0$, and (3) $\boldsymbol{\theta}_A^{(A)} = \mathbf{0}$ or $\boldsymbol{\theta}_A^{(B)} = \mathbf{0}$, and $\boldsymbol{\theta}_B^{(A)} = \mathbf{0}$ or $\boldsymbol{\theta}_B^{(B)} = \mathbf{0}$. However, all except two of these solutions produce trivial features and increase the classification error. The only remaining non-degenerate solutions are: (S1) $\boldsymbol{\theta}_A^{(A)} = \mathbf{0}, \boldsymbol{\theta}_B^{(B)} = \mathbf{0}$, and (S2) $\boldsymbol{\theta}_B^{(A)} = \mathbf{0}, \boldsymbol{\theta}_A^{(B)} = \mathbf{0}$. Note that (S2) corresponds to a robust model. Since both (S1) and (S2) minimize Eq. (4), the solution that minimizes the prediction error on both A and B during training will prevail.

Proposition 1. *The total training error for (S1) is strictly greater than that of (S2) when the following conditions are satisfied: (1)* $\beta \geq 1 - \frac{1}{|w_{AB}|}$*, (2)* $\beta \geq \min\left(\frac{\rho_A^2}{2\rho_{B'}^2+\rho_A^2}, \frac{\rho_{\boldsymbol{U}_A}^2}{w_A^2 w_{AB}^2 \rho_A^2}\right)$.

Proposition 1 states that a robust model is guaranteed when a minimum amount of interventional data is available during training. Note that Proposition 1 describes sufficient conditions for (S1) to have a larger training error than (S2). In practice, β could be smaller. Refer to App. B.3 for a detailed derivation and experimental verification of Proposition 1.

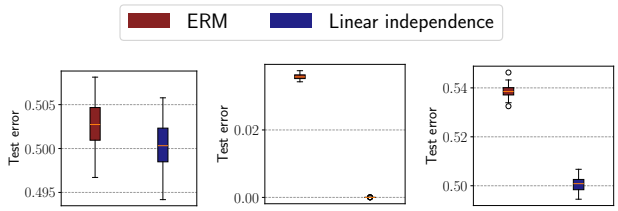

(a) $E_A^{(1)}$ (b) $E_A^{(2)}$ (c) E_A

Figure 4: Robust models achieve $E_A^{(2)} = 0$ in Eq. (1). ERM models have a non-zero $\boldsymbol{\theta}_B^{(A)}$ resulting in $E_A^{(2)} \neq 0$. Minimizing linear independence on interventional features results in orthogonal interventional feature spaces where $\boldsymbol{\theta}_B^{(A)} = \boldsymbol{\theta}_A^{(B)} = \mathbf{0}$. Thus, they result in robust models with $E_A^{(2)} = 0$.

Experimental verification: To experimentally verify the theoretical results, we simulate the causal model by setting $w_A = w_B = w_{AB} = 1$. The random variables A, B, U_A, and U_B are sampled from independent normal distributions with zero mean and unit variance. We generate $N = 50000$ data points for training with $\beta = 0.5$. The classifiers use 2-dimensional features learned by linear feature extractors to predict A and B. The experiment is repeated with 50 seeds. In Eq. (1), the statistical risk was shown to be composed of $E_A^{(1)}$ and $E_A^{(2)}$, plotted in Figs. 4a and 4b respectively. An ideal robust model will achieve $E_A^{(2)} = 0$. As expected, both models have similar $E_A^{(1)}$. However, linear independence models minimize $E_A^{(2)}$, resulting in a lower total error E_A shown in Fig. 4c.

[3]For a complete definition of the dependence, refer to App. B.3.

4 RepLIn: Enforcing Statistical Independence between Interventional Features

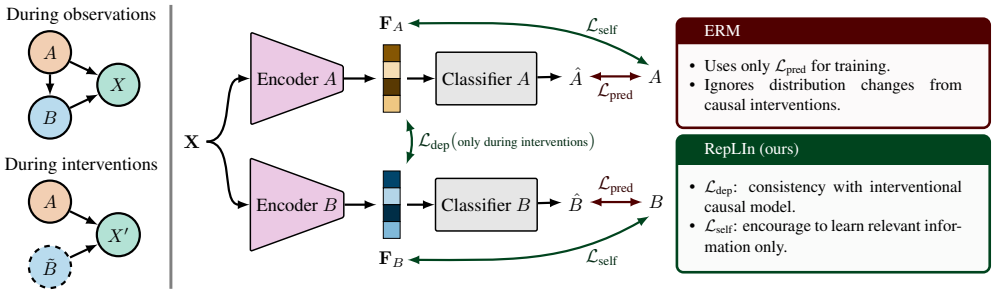

Figure 5: Schematic illustration of **RepLIn** for a causal graph with two attributes ($A \to B$) and $\boldsymbol{X} = f(A, B, \boldsymbol{U})$. Encoders learn representations $\boldsymbol{F}_A$ and $\boldsymbol{F}_B$ corresponding to A and B, which are then used by their corresponding classifiers to predict $\hat{A}$ and $\hat{B}$ respectively. On interventional samples, we minimize $\mathcal{L}_{\text{dep}}$ between the features to ensure their independence. On all samples, we minimize $\mathcal{L}_{\text{self}}$ to encourage the representations to learn only the relevant information.

As noted in the previous section, there is a strong correlation between the drop in accuracy during interventions and interventional feature dependence. We also showed theoretically that minimizing linear dependence between interventional features can improve test time error on interventional data for linear models. Based on this observation, we propose "Representation Learning from Interventional data" (RepLIn) to learn discriminative representations that are robust against interventional distribution shifts.

To enforce independence between interventional features, we propose to use dependence-guided regularization denoted as $\mathcal{L}_{\text{dep}}$ over the prediction loss function (e.g., cross-entropy for classification tasks) used in ERM. We refer to this regularization as "dependence loss" and is defined for the general case in Sec. 3 as $\mathcal{L}_{\text{dep}} = \sum_{i=1}^{n} \text{NHSIC}(\boldsymbol{F}_{A_i}^{\text{int}}, \boldsymbol{F}_B^{\text{int}})$. We minimize the dependence loss *only* for the interventional samples in our training set since congruent statistical independence occurs in the data space only during interventions.

However, $\mathcal{L}_{\text{dep}}$ alone is insufficient since learning irrelevant features can minimize $\mathcal{L}_{\text{dep}}$. To avoid such pathological scenarios and encourage the model to learn only relevant information, we introduce another loss that maximizes the dependence between a feature and its corresponding label. We employ this "self-dependence loss" on both observational and interventional data and define it as $\mathcal{L}_{\text{self}} = 1 - \frac{\text{NHSIC}(\boldsymbol{F}_B, B) + \sum_{i=1}^{n} \text{NHSIC}(\boldsymbol{F}_{A_i}, A_i)}{2(n+1)}$. However, in contrast to $\mathcal{L}_{\text{dep}}$, we use linear kernels in $\mathcal{L}_{\text{self}}$ to maximize a lower estimate of the dependence between the representations and the labels. Using linear kernels in HSIC amounts to $k_P\left(\boldsymbol{x}^{(i)}, \boldsymbol{x}^{(j)}\right) = \boldsymbol{x}^{(i)\top}\boldsymbol{x}^{(j)}$ in Sec. 3.2. In summary, RepLIn optimizes the following total loss: $\mathcal{L}_{\text{total}} = \mathcal{L}_{\text{pred}} + \lambda_{\text{dep}}\mathcal{L}_{\text{dep}} + \lambda_{\text{self}}\mathcal{L}_{\text{self}}$, where λ_{dep} and λ_{self} are weights that control the contribution of the respective losses. A pictorial overview of the RepLIn pipeline is shown in Fig. 5.

5 Experimental Evaluation

In this section, we compare the performance of RepLIn to the baselines on synthetic and real face image datasets. We use the Windmill dataset introduced in Sec. 3.1 to verify the effectiveness of RepLIn and evaluate its broader applicability to practical scenarios through the facial attribute prediction task on the CelebA dataset. Our experiments are designed to validate the following hypothesis: *Does explicitly minimizing the interventional feature dependence improve interventional accuracy?*

Training Hyperparameters and Baselines: We consider vanilla ERM and ERM-Resampled (Chawla et al., 2002; Cateni et al., 2014) as our primary baselines since they are the most commonly used training algorithms. ERM-Resampled is a strong baseline for group-imbalanced training and domain generalization (Idrissi et al., 2022; Gulrajani & Lopez-Paz, 2021). On Windmill dataset, we also consider the following SOTA algorithms in domain generalization: IRMv1 (Arjovsky et al., 2019), Fish (Shi et al., 2022), and GroupDRO (Sagawa et al., 2020). We study two variants of our method: RepLIn and RepLIn-Resampled.

The latter variant uses the resampling strategy from ERM-Resampled. In each method, attribute-specific representations are extracted from the input data, which feed into the classifiers to get the final prediction. All baselines share the same architecture for feature extractors. Linear classifiers are used for all baselines. We note that the values of λ_{dep} and λ_{self} in RepLIn variants are kept fixed across all proportions of interventional data β. A detailed description of the datasets and the training settings is provided in App. A.

Evaluation Criterion: Our primary interest is in investigating the accuracy drop when predicting the variables that are unaffected by interventions. Ideally, if the learned features respect causal relations during interventions, we expect no change in the prediction accuracy of parent variables of the intervened variable between observational and interventional distributions. To measure the change, we use the relative drop in accuracy defined in Sec. 3.3: $\text{Rel.}\Delta = \frac{\text{Obs acc.} - \text{Int acc.}}{\text{Obs acc.}}$. Since we optimize NHSIC during training, we use NKCC from Sec. 3.3 to evaluate the dependence between the features on interventional data during testing. We repeat each experiment with five different random seeds and report the mean and standard deviation.

5.1 Windmill dataset

We first evaluate our method on the synthetic dataset that helped us identify the relation between the performance gap in predicting A on observational and interventional data in Sec. 3.1. As a reminder, the causal graph consists of two binary random variables A and B, where $A \to B$ during observations. We intervene by setting $B \sim \text{Bernoulli}(0.5)$, breaking the dependence between A and B. The proportion of interventional samples in the training data varies from $\beta = 0.01$ to $\beta = 0.5$.

Accuracy on interventional data. The relative drop in accuracy is shown in parentheses.

Method	$\beta = 0.5$		$\beta = 0.3$		$\beta = 0.1$		$\beta = 0.05$		$\beta = 0.01$	
ERM	76.87 ± 1.08	(0.18 ± 0.01)	69.86 ± 3.19	(0.29 ± 0.04)	62.78 ± 1.77	(0.37 ± 0.02)	59.52 ± 1.30	(0.40 ± 0.01)	60.15 ± 3.12	(0.40 ± 0.03)
ERM-Resampled	73.70 ± 3.19	(0.22 ± 0.04)	71.19 ± 3.23	(0.24 ± 0.03)	73.62 ± 1.54	(0.22 ± 0.02)	71.03 ± 2.83	(0.25 ± 0.03)	70.20 ± 3.73	(0.26 ± 0.03)
IRMv1	78.24 ± 0.79	(0.16 ± 0.01)	74.83 ± 1.74	(0.20 ± 0.02)	78.61 ± 2.24	(0.16 ± 0.02)	76.28 ± 1.87	(0.18 ± 0.02)	71.75 ± 2.03	(0.24 ± 0.02)
Fish	77.23 ± 2.24	(0.19 ± 0.02)	77.23 ± 1.32	(0.19 ± 0.01)	78.24 ± 2.09	(0.18 ± 0.02)	76.42 ± 1.95	(0.20 ± 0.02)	**73.92 ± 2.53**	(0.23 ± 0.03)
GroupDRO	80.10 ± 1.66	**(0.02 ± 0.01)**	80.96 ± 1.33	**(0.04 ± 0.02)**	80.35 ± 1.01	**(0.06 ± 0.02)**	**77.40 ± 1.16**	**(0.08 ± 0.01)**	71.86 ± 1.60	**(0.22 ± 0.02)**
RepLIn	**87.94 ± 1.46**	(0.08 ± 0.02)	**87.76 ± 2.30**	(0.10 ± 0.02)	**83.23 ± 2.67**	(0.16 ± 0.03)	73.63 ± 2.43	(0.25 ± 0.02)	67.52 ± 2.30	(0.32 ± 0.03)
RepLIn-Resampled	**88.46 ± 0.96**	**(0.07 ± 0.01)**	**88.05 ± 1.04**	**(0.08 ± 0.01)**	**87.91 ± 1.36**	**(0.08 ± 0.01)**	**86.38 ± 0.85**	**(0.10 ± 0.01)**	**78.41 ± 1.27**	**(0.18 ± 0.02)**

Table 2: **Results on Windmill dataset:** We evaluate the variants of RepLIn (highlighted in gray) against the baselines on two metrics: interventional accuracy and relative accuracy drop on interventional data compared to observational. As the proportion of interventional data during training (β) decreases, the problem becomes more challenging. Compared to the baselines, RepLIn maintains its interventional accuracy. A similar trend is observed in the relative accuracy drop, where RepLIn significantly outperforms most baselines. The **best** and the **second-best** results are shown in different colors.

Tab. 2 compares the interventional accuracy of A for various amounts of interventional data. We make the following observations: **(1)** our model outperforms every baseline in interventional accuracy for all values of β. This clearly demonstrates the advantage of exploiting the underlying causal relations when learning from interventional data, instead of treating it as a separate domain, and **(2)** comparing ERM and RepLIn with their resampling variants, we observe that resampling is a generally useful technique with large gains when β is very small (for example, consider results with $\beta \leq 0.05$). We are also interested in the relative drop in accuracy between observational and interventional data (Rel.Δ). From Tab. 2, we observe that GroupDRO has the lowest Rel.Δ among the considered methods for $\beta \geq 0.05$, and achieves its best results when more interventional data is available during training. However, this improvement comes at the cost of lower interventional accuracy. Meanwhile, the relative drop in accuracy of RepLIn is comparable to GroupDRO at larger values of β and has the least relative drop in accuracy at lower values of β. We discuss in Sec. 6.1 how the representations learned by RepLIn are less affected by interventional shifts.

5.2 Facial Attribute Prediction

We verify the utility of RepLIn for predicting facial attributes on the CelebA dataset (Liu et al., 2015). Images in the CelebA dataset are annotated with 40 labeled binary attributes. We consider two of these attributes – `smiling` and `gender` – as random variables affecting each other causally. Since the true underlying relation between smile and gender is unknown, we adopt the resampling procedure from (Wang & Boddeti,

2022) to induce a desired causal relation between the attributes (`smiling` → `gender`) and obtain samples. Specifically, to simulate this causal relation, we sample `smiling` from Bernoulli(0.6) first and then sample `gender` according to a probability distribution conditioned on the sampled `smiling` variable. We then sample a face image whose attribute labels match the sampled values. We model the diversity in the images due to unobserved noise variables. Note that, unlike in WINDMILL, the noise variables in this experiment *may be* causally related to the attributes that we wish to predict, adding to the challenges in the dataset. The causal model for this experiment and some sample images are shown in Fig. 7.

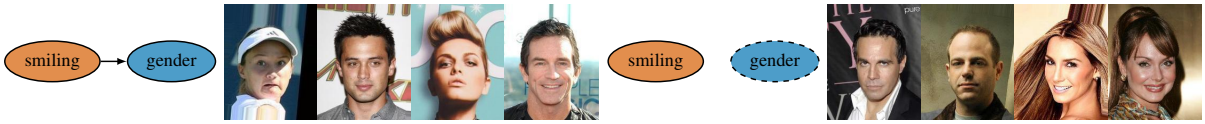

(a) Observational causal graph and samples (b) Interventional causal graph and samples

Figure 7: Causal model for CelebA before and after intervention along with sample images from these models

Given the face images, we first extract features from ResNet-50 (He et al., 2016) pre-trained on ImageNet dataset (Deng et al., 2009). Then, similar to the architecture for WINDMILL experiments, we employ a shallow MLP to act on these features, followed by a linear classifier to predict the attributes. Our loss functions act upon the features of the MLP. We use 30,000 samples for training and 15,000 for testing. We use the relative drop in interventional accuracy as the primary metric and compare RepLIn-Resampled against ERM-Resampled. We also verify if the correlation between interventional feature dependence and the relative drop in accuracy observed in Sec. 3.3 on WINDMILL experiments holds in a more practical scenario.

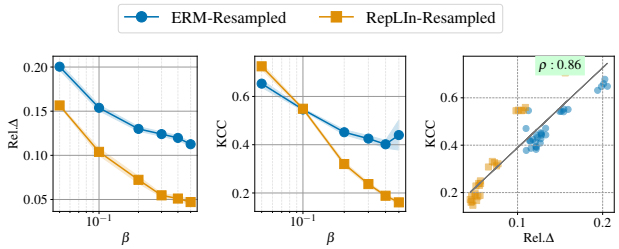

(a) Accuracy (b) Dependence (c) Correlation

Figure 8: **Facial Attribute Prediction:** (a) RepLIn has a lower relative drop in accuracy compared to ERM-Resampled. (b) Minimizing interventional feature dependence during training generalizes to testing. (c) Interventional feature dependence correlates positively with the relative drop in accuracy.

Fig. 8 reports the experimental results on facial attribute prediction for various amounts of interventional training data. We make the following observations: **(1)** as the proportion of interventional data increases, the relative drop in accuracy in all methods decreases, **(2)** across all proportions of interventional data, RepLIn consistently outperforms the baseline by $4\% - 7\%$ lower relative drop in accuracy despite the potential challenges due to noise variable being causally related to the attributes of interest, **(3)** relative drop in accuracy and interventional feature dependence show strong positive correlation ($\rho = 0.86$), and **(4)** the interventional feature dependence of RepLIn steadily decreases as the amount of interventional data increases.

6 Discussion

6.1 How does RepLIn improve robustness against interventional distribution shift?

In Sec. 3.4, we showed theoretically that enforcing linear independence between interventional features can improve robustness in a linear model. We verified our claims experimentally in non-linear settings in Sec. 5. In this section, we qualitatively and quantitatively compare the interventional features learned by various methods to understand how RepLIn improves robustness against interventional distribution shift.

Windmill dataset: We consider the distribution of $\boldsymbol{F}_A^{\text{int}}$ for a fixed value of A and changing values of B. Robust representations of A change with A but not B. The distribution shift in $\boldsymbol{F}_A^{\text{int}}$ due to changes in B can be quantitatively measured using Jensen-Shannon (JS) divergence. In Tab. 3, we calculate JS

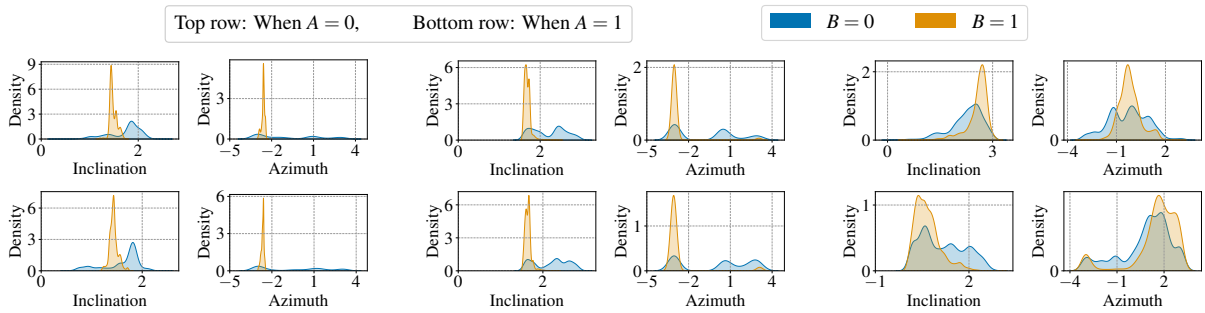

(a) ERM (b) ERM-Resampled (c) RepLIn-Resampled

Figure 9: Visualization of interventional features learned by various methods on WINDMILL dataset.

Method	ERM	ERM-Resampled	IRMv1	Fish	GroupDRO	RepLIn	RepLIn-Resampled
When $A = 0$	0.45 ± 0.058	0.423 ± 0.105	0.333 ± 0.122	0.341 ± 0.111	0.365 ± 0.066	**0.15 ± 0.03**	**0.188 ± 0.032**
When $A = 1$	0.499 ± 0.07	0.456 ± 0.11	0.405 ± 0.111	0.37 ± 0.116	0.431 ± 0.048	**0.183 ± 0.058**	**0.168 ± 0.047**
Average	0.475 ± 0.063	0.439 ± 0.105	0.369 ± 0.116	0.355 ± 0.113	0.398 ± 0.055	**0.166 ± 0.035**	**0.178 ± 0.036**

Table 3: **Jensen-Shannon (JS) divergence:** The distribution of $\boldsymbol{F}_A^{\text{int}}$ must be invariant to the value assumed by B since $A \perp\!\!\!\perp B$ during interventions. Therefore, JS divergence between $P(\boldsymbol{F}_A^{\text{int}}|B = 0, A = a)$ and $P(\boldsymbol{F}_A^{\text{int}}|B = 1, A = a)$ of a robust model must be zero. We compare the JS divergence between interventional features of the baselines for $\beta = 0.5$. Among the baselines, RepLIn achieves the lowest values of Jensen-Shannon divergence. The lowest and the second lowest scores are highlighted in color.

divergence between $P(\boldsymbol{F}_A^{\text{int}}|B = 0, A = a)$ and $P(\boldsymbol{F}_A^{\text{int}}|B = 1, A = a)$ for all methods trained on WINDMILL dataset. JS divergence for an ideal robust model must be zero. We observe that $\boldsymbol{F}_A^{\text{int}}$ learned by RepLIn achieves the lowest JS divergence. This shows that $\boldsymbol{F}_A^{\text{int}}$ learned by RepLIn contains the least information about B among the baselines. In our experiments on WINDMILL dataset, all baselines learned 3-dimensional features that lay on a unit radius sphere. Therefore, we can visualize the distributions of their spherical angles, namely inclination and azimuth. We compare the distributions of inclination and azimuth of $\boldsymbol{F}_A^{\text{int}}$ learned by RepLIn-Resampled against the ERM baselines in Fig. 9. Each row shows the distribution of the spherical angles for different values of A. Distributions for different values of B have separate colors. These feature distributions for a robust model must change with A but not B. We observed from the figure that the feature distributions of the baselines are affected by B and not A due to the dependence between $\boldsymbol{F}_A^{\text{int}}$ and B. However, the feature distributions learned by RepLIn change with A and overlap significantly when B takes different values. Thus, our models perform similarly to a robust model. Visualizations of the feature distributions of other baselines are provided in App. E.

(a) ERM-Resampled

(b) RepLIn-Resampled

Figure 10: Consider these sample face images where the subjects are smiling. The ERM baseline misclassified these samples as not smiling, while RepLIn classified them correctly. We use GradCAM visualizations to identify the regions in the input images that the models used to make their predictions. The ERM model relied on factors such as hair and the presence of a hat that may correlate with gender to predict whether the subjects are smiling. In contrast, RepLIn attended to the lip regions to make predictions.

CelebA dataset: Our learned representations on CelebA are high-dimensional, and therefore we employ Grad-CAM (Selvaraju et al., 2017) to analyze the features and compare them against those learned by ERM-Resampled. Since our primary metric is accuracy in predicting `smiling` during interventions, we visualize

the parts of the input image that the models attend to for predicting a smile. We consider some samples with `smiling` $= 1$ that were misclassified by ERM-Resampled but were correctly classified by RepLIn-Resampled. Comparing these predictions would help us explain the robustness of RepLIn. Fig. 10 shows the attention maps from models trained on datasets with 50% interventional data. A robust model would attend to facial regions surrounding lips to make predictions about smiling. Observe that RepLIn-Resampled tends to focus more on the region around the lips while ERM-Resampled attends to other regions of the face.

6.2 Scalability with number of nodes

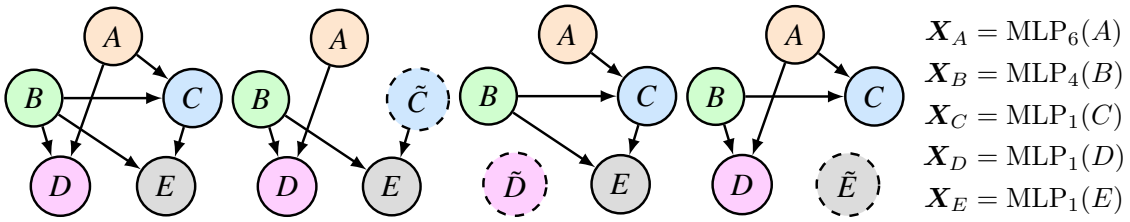

(a) Observational (b) Intervening on C (c) Intervening on D (d) Intervening on E (e) Generating $\boldsymbol{X}$

Figure 11: **5-variable causal graph**: We construct a 5-variable causal graph to demonstrate the scalability of our method with the number of nodes. To collect interventional data, we intervene on C, D, and E separately and measure the performance drop in predicting A and B during these interventions. Nodes in the graphs with dashed borders indicate intervened nodes. Note that we do not intervene on multiple targets at a time. The input data signal $\boldsymbol{X}$ is constructed as a concatenation of individual input signals, each being a function of a latent variable, i.e., $\boldsymbol{X} = \begin{bmatrix}\boldsymbol{X}_A^\top & \boldsymbol{X}_B^\top & \boldsymbol{X}_C^\top & \boldsymbol{X}_D^\top & \boldsymbol{X}_E^\top\end{bmatrix}^\top$ Here, MLP_l indicates a randomly initialized MLP with l linear layers, each followed by a ReLU. We also add Gaussian noise sampled from $\mathcal{N}(0, 0.01)$ to the output of the MLP.

Consider a causal graph with N nodes, each with K parent nodes. To learn robustness against distribution shifts due to interventions on M nodes, RepLIn requires only the independence relations between these M nodes and their parents and the data resulting from separate interventions on these nodes. Therefore, RepLIn can scale with M and K. To verify this scalability, we use the causal graph shown in Fig. 11a with five latent variables. It consists of two binary source nodes A and B, and three binary derived nodes C, D, and E. During observations, A and B are sampled from independent Bernoulli(0.5) distributions. During observation, the remaining nodes take the following logical expressions: $C \coloneqq A$ `or` B, $D \coloneqq A$ `and` B, and $E \coloneqq$ `not` B `and` C. Like our previous experiments, the training dataset has interventional data samples collected by intervening on nodes C, D, and E separately in addition to the observational data. The changes in the causal graph due to these interventions are shown in Figs. 11b to 11d. Each intervened variable assumes values from a Bernoulli(0.5) distribution independent of their parents. Each latent variable $*$ is passed through a randomly initialized MLP with noise added to its output to get a corresponding observed signal $\boldsymbol{X}_*$. These individual signals are concatenated to obtain the observed input signal $\boldsymbol{X}$, as shown in Fig. 11e. The task is to predict the latent variables from the input signal $\boldsymbol{X}$. Since we are interested in the robustness of the model against interventional distribution shift, our primary metrics will be the predictive accuracy for A and B during interventions on C, D, and E.

Each batch comprises only observational or interventional data after intervention on a single target. Therefore, our method only enforces the independence relations from at most one interventional target in each batch. The validation and test sets consist of samples collected during interventions on C, D, or E. The predictive performances on the test sets are reported in Table 4. We observe that RepLIn significantly improves over the baseline with sufficient interventional data, $\beta > 0.1$. When the proportion of interventional data $\beta \leq 0.1$, RepLIn is comparable with the baseline, suggesting that the benefits of enforcing independence between interventional features extend to larger causal graphs with multiple intervention targets.

Interventional target	Method	Predictive accuracy on A				Predictive accuracy on B			
		$\beta = 0.5$	$\beta = 0.3$	$\beta = 0.1$	$\beta = 0.05$	$\beta = 0.5$	$\beta = 0.3$	$\beta = 0.1$	$\beta = 0.05$
C	ERM-Resampled	79.71 ± 0.30	76.22 ± 0.42	$\mathbf{73.97 \pm 0.39}$	73.56 ± 0.36	87.60 ± 0.06	85.45 ± 0.23	$\mathbf{83.89 \pm 0.33}$	$\mathbf{83.71 \pm 0.40}$
	RepLIn-Resampled	$\mathbf{95.37 \pm 0.97}$	$\mathbf{78.77 \pm 0.54}$	72.15 ± 0.31	$\mathbf{73.74 \pm 0.36}$	$\mathbf{96.72 \pm 0.81}$	$\mathbf{86.16 \pm 0.63}$	82.35 ± 0.95	82.43 ± 0.65
D	ERM-Resampled	79.65 ± 0.43	75.47 ± 0.64	$\mathbf{71.76 \pm 0.35}$	$\mathbf{70.27 \pm 0.34}$	91.05 ± 0.29	90.21 ± 0.27	90.36 ± 0.58	90.55 ± 0.74
	RepLIn-Resampled	$\mathbf{95.49 \pm 1.01}$	$\mathbf{77.76 \pm 0.82}$	71.20 ± 0.82	68.80 ± 0.79	$\mathbf{97.87 \pm 0.31}$	$\mathbf{92.21 \pm 0.48}$	$\mathbf{91.40 \pm 0.79}$	$\mathbf{90.88 \pm 0.89}$
E	ERM-Resampled	86.63 ± 0.33	81.90 ± 0.26	$\mathbf{76.20 \pm 0.84}$	$\mathbf{73.46 \pm 0.37}$	81.12 ± 0.22	78.00 ± 0.48	$\mathbf{74.02 \pm 0.38}$	$\mathbf{72.97 \pm 0.38}$
	RepLIn-Resampled	$\mathbf{96.71 \pm 0.49}$	$\mathbf{84.68 \pm 0.36}$	75.01 ± 0.53	71.52 ± 0.87	$\mathbf{96.89 \pm 0.68}$	$\mathbf{80.88 \pm 0.57}$	72.81 ± 1.13	71.60 ± 0.59

Table 4: **Results on 5-variable causal graph:** We compare the accuracy of RepLIn in predicting the source nodes A and B during interventions on non-source nodes C, D, and E against that of ERM-Resampled. Our approach outperforms the baselines with sufficient interventional data.

7 Conclusion

This paper considered the problem of learning representations that are robust against interventional distribution shifts by leveraging the statistical independence induced by interventions in the underlying data-generating process. First, we established a strong correlation between the drop in accuracy during interventions and statistical dependence between representations on interventional data. We then showed theoretically that minimizing linear dependence between interventional representations can improve the robustness of a linear model against interventional distribution shift. Building on this result, we proposed RepLIn to learn representations that are robust against interventional distribution shift by explicitly enforcing statistical independence between learned representations on interventional data. Experimental evaluation of RepLIn across different scenarios corresponding to different causal graphs showed that RepLIn can improve predictive accuracy during interventions for various proportions of interventional data. RepLIn is also scalable to the number of causal attributes and can be used with continuous and discrete latent variables. We used qualitative and quantitative tools to show that RepLIn is more successful in learning interventional representations that do not contain information about their child nodes during interventions.

References

Kartik Ahuja, Jason S Hartford, and Yoshua Bengio. Weakly supervised representation learning with sparse perturbations. In *Advances in Neural Information Processing Systems*, 2022a. URL https://papers.nips.cc/paper_files/paper/2022/hash/63d3bae2c1f525745003f679e45bcf7b-Abstract-Conference.html.

Kartik Ahuja, Divyat Mahajan, Vasilis Syrgkanis, and Ioannis Mitliagkas. Towards efficient representation identification in supervised learning. In *Conference on Causal Learning and Reasoning*, pp. 19–43. PMLR, 2022b.

Kartik Ahuja, Yixin Wang, Divyat Mahajan, and Yoshua Bengio. Interventional causal representation learning. In *International Conference on Machine Learning*, 2023.

Martin Arjovsky, Léon Bottou, Ishaan Gulrajani, and David Lopez-Paz. Invariant risk minimization. *arXiv preprint arXiv:1907.02893*, 2019. URL https://arXiv.org/abs/1907.02893.

Francis R Bach and Michael I Jordan. Kernel independent component analysis. *Journal of Machine Learning Research*, 3(Jul):1–48, 2002.

Johann Brehmer, Pim De Haan, Phillip Lippe, and Taco Cohen. Weakly supervised causal representation learning. In *Advances in Neural Information Processing Systems*, 2022.

Philippe Brouillard, Sébastien Lachapelle, Alexandre Lacoste, Simon Lacoste-Julien, and Alexandre Drouin. Differentiable causal discovery from interventional data. In *Advances in Neural Information Processing Systems*, 2020.

Tom Brown, Benjamin Mann, Nick Ryder, Melanie Subbiah, Jared D Kaplan, Prafulla Dhariwal, Arvind Neelakantan, Pranav Shyam, Girish Sastry, Amanda Askell, et al. Language models are few-shot learners. In *Advances in Neural Information Processing Systems*, 2020.

Silvia Cateni, Valentina Colla, and Marco Vannucci. A method for resampling imbalanced datasets in binary classification tasks for real-world problems. *Neurocomputing*, 135:32–41, 2014.

Nitesh V Chawla, Kevin W Bowyer, Lawrence O Hall, and W Philip Kegelmeyer. Smote: Synthetic minority over-sampling technique. *Journal of Artificial Intelligence Research*, 16:321–357, 2002.

Mostafa Dehghani, Josip Djolonga, Basil Mustafa, Piotr Padlewski, Jonathan Heek, Justin Gilmer, Andreas Peter Steiner, Mathilde Caron, Robert Geirhos, Ibrahim Alabdulmohsin, et al. Scaling vision transformers to 22 billion parameters. In *International Conference on Machine Learning*, 2023.

Jia Deng, Wei Dong, Richard Socher, Li-Jia Li, Kai Li, and Li Fei-Fei. Imagenet: A large-scale hierarchical image database. In *IEEE/CVF Conference on Computer Vision and Pattern Recognition*, 2009.

Wenhao Ding, Haohong Lin, Bo Li, and Ding Zhao. Generalizing goal-conditioned reinforcement learning with variational causal reasoning. In *Advances in Neural Information Processing Systems*, 2022.

Frederick Eberhardt, Clark Glymour, and Richard Scheines. On the number of experiments sufficient and in the worst case necessary to identify all causal relations among n variables. In *Conference on Uncertainty in Artificial Intelligence*, 2005.

Tongtong Fang, Nan Lu, Gang Niu, and Masashi Sugiyama. Rethinking importance weighting for deep learning under distribution shift. In *Advances in Neural Information Processing Systems*, 2020.

Irena Gao, Shiori Sagawa, Pang Wei Koh, Tatsunori Hashimoto, and Percy Liang. Out-of-domain robustness via targeted augmentations. In *International Conference on Machine Learning*, 2023.

Maxime Gasse, Damien Grasset, Guillaume Gaudron, and Pierre-Yves Oudeyer. Causal reinforcement learning using observational and interventional data. *arXiv preprint arXiv:2106.14421*, 2021.

Arthur Gretton, Olivier Bousquet, Alex Smola, and Bernhard Schölkopf. Measuring statistical dependence with hilbert-schmidt norms. In *International conference on algorithmic learning theory*, pp. 63–77. Springer, 2005.

Ishaan Gulrajani and David Lopez-Paz. In search of lost domain generalization. In *International Conference on Learning Representations*, 2021. URL `https://openreview.net/forum?id=lQdXeXDoWtI`.

Kaiming He, Xiangyu Zhang, Shaoqing Ren, and Jian Sun. Deep residual learning for image recognition. In *IEEE/CVF Conference on Computer Vision and Pattern Recognition*, 2016.

Christina Heinze-Deml and Nicolai Meinshausen. Conditional variance penalties and domain shift robustness. *Machine Learning*, 110(2):303–348, 2021.

Aapo Hyvarinen and Hiroshi Morioka. Unsupervised feature extraction by time-contrastive learning and nonlinear ica. In *Advances in Neural Information Processing Systems*, volume 29, 2016.

Aapo Hyvarinen, Hiroaki Sasaki, and Richard Turner. Nonlinear ica using auxiliary variables and generalized contrastive learning. In *The 22nd International Conference on Artificial Intelligence and Statistics*, 2019.

Aapo Hyvärinen, Ilyes Khemakhem, and Ricardo Monti. Identifiability of latent-variable and structural-equation models: from linear to nonlinear. *Annals of the Institute of Statistical Mathematics*, 76(1):1–33, 2024.

Badr Youbi Idrissi, Martin Arjovsky, Mohammad Pezeshki, and David Lopez-Paz. Simple data balancing achieves competitive worst-group-accuracy. In *Conference on Causal Learning and Reasoning*, 2022. URL `https://proceedings.mlr.press/v177/idrissi22a.html`.

Nan Rosemary Ke, Olexa Bilaniuk, Anirudh Goyal, Stefan Bauer, Hugo Larochelle, Bernhard Schölkopf, Michael C Mozer, Chris Pal, and Yoshua Bengio. Learning neural causal models from unknown interventions. *arXiv preprint arXiv:1910.01075*, 2019.

Nan Rosemary Ke, Silvia Chiappa, Jane Wang, Jorg Bornschein, Theophane Weber, Anirudh Goyal, Matthew Botvinic, Michael Mozer, and Danilo Jimenez Rezende. Learning to induce causal structure. In *International Conference on Learning Representattions*, 2022.

Maurice G Kendall. A new measure of rank correlation. *Biometrika*, 30(1/2):81–93, 1938.

Ilyes Khemakhem, Diederik Kingma, Ricardo Monti, and Aapo Hyvarinen. Variational autoencoders and nonlinear ica: A unifying framework. In *International Conference on Artificial Intelligence and Statistics*, 2020.

Diederik P Kingma and Jimmy Ba. Adam: A method for stochastic optimization. In *International Conference on Learning Representations*, 2015.

David Klindt, Lukas Schott, Yash Sharma, Ivan Ustyuzhaninov, Wieland Brendel, Matthias Bethge, and Dylan Paiton. Towards nonlinear disentanglement in natural data with temporal sparse coding. In *International Conference on Learning Representations*, 2021.

Lingjing Kong, Shaoan Xie, Weiran Yao, Yujia Zheng, Guangyi Chen, Petar Stojanov, Victor Akinwande, and Kun Zhang. Partial identifiability for domain adaptation. In *International Conference on Machine Learning*, 2022. URL `https://proceedings.mlr.press/v162/kong22a.html`.

Karl Krauth, Yixin Wang, and Michael I Jordan. Breaking feedback loops in recommender systems with causal inference. *arXiv preprint arXiv:2207.01616*, 2022.

Sébastien Lachapelle, Pau Rodriguez, Yash Sharma, Katie E Everett, Rémi Le Priol, Alexandre Lacoste, and Simon Lacoste-Julien. Disentanglement via mechanism sparsity regularization: A new principle for nonlinear ica. In *Conference on Causal Learning and Reasoning*, 2022.

Yazhe Li, Roman Pogodin, Danica J Sutherland, and Arthur Gretton. Self-supervised learning with kernel dependence maximization. In *Advances in Neural Information Processing Systems*, 2021.

Phillip Lippe, Taco Cohen, and Efstratios Gavves. Efficient neural causal discovery without acyclicity constraints. In *International Conference on Learning Representations*, 2022a.

Phillip Lippe, Sara Magliacane, Sindy Löwe, Yuki M Asano, Taco Cohen, and Stratis Gavves. Citris: Causal identifiability from temporal intervened sequences. In *International Conference on Machine Learning*, 2022b.

Phillip Lippe, Sara Magliacane, Sindy Löwe, Yuki M Asano, Taco Cohen, and Efstratios Gavves. Causal representation learning for instantaneous and temporal effects in interactive systems. In *International Conference on Learning Representations*, 2023.

Ziwei Liu, Ping Luo, Xiaogang Wang, and Xiaoou Tang. Deep learning face attributes in the wild. In *IEEE/CVF International Conference on Computer Vision*, 2015.

Francesco Locatello, Stefan Bauer, Mario Lucic, Gunnar Raetsch, Sylvain Gelly, Bernhard Schölkopf, and Olivier Bachem. Challenging common assumptions in the unsupervised learning of disentangled representations. In *International Conference on Machine Learning*, pp. 4114–4124. PMLR, 2019.

Chaochao Lu, Yuhuai Wu, José Miguel Hernández-Lobato, and Bernhard Schölkopf. Invariant causal representation learning for out-of-distribution generalization. In *International Conference on Learning Representations*, 2021.

Huishi Luo, Fuzhen Zhuang, Ruobing Xie, Hengshu Zhu, Deqing Wang, Zhulin An, and Yongjun Xu. A survey on causal inference for recommendation. *The Innovation*, 2024.

Gemma Elyse Moran, Dhanya Sridhar, Yixin Wang, and David Blei. Identifiable deep generative models via sparse decoding. *Transactions on Machine Learning Research*, 2022. URL `https://openreview.net/forum?id=vd0onGWZbE`.

Adam Paszke, Sam Gross, Francisco Massa, Adam Lerer, James Bradbury, Gregory Chanan, Trevor Killeen, Zeming Lin, Natalia Gimelshein, Luca Antiga, et al. Pytorch: An imperative style, high-performance deep learning library. In *Advances in Neural Information Processing Systems*, 2019.

Judea Pearl. *Causality*. Cambridge University Press, 2009.

Jonas Peters, Dominik Janzing, and Bernhard Schölkopf. *Elements of Causal Inference: Foundations and Learning Algorithms*. The MIT Press, 2017.

Alec Radford, Jong Wook Kim, Chris Hallacy, Aditya Ramesh, Gabriel Goh, Sandhini Agarwal, Girish Sastry, Amanda Askell, Pamela Mishkin, Jack Clark, et al. Learning transferable visual models from natural language supervision. In *International Conference on Machine Learning*, 2021.

Sorawit Saengkyongam and Ricardo Silva. Learning joint nonlinear effects from single-variable interventions in the presence of hidden confounders. In *Conference on Uncertainty in Artificial Intelligence*, 2020.

Sorawit Saengkyongam, Elan Rosenfeld, Pradeep Ravikumar, Niklas Pfister, and Jonas Peters. Identifying representations for intervention extrapolation. In *International Conference on Learning Representations*, 2024.

Shiori Sagawa, Pang Wei Koh, Tatsunori B Hashimoto, and Percy Liang. Distributionally robust neural networks for group shifts: On the importance of regularization for worst-case generalization. In *International Conference on Learning Representations*, 2020.

Axel Sauer and Andreas Geiger. Counterfactual generative networks. In *International Conference on Learning Representations*, 2021.

Bernhard Schölkopf, Francesco Locatello, Stefan Bauer, Nan Rosemary Ke, Nal Kalchbrenner, Anirudh Goyal, and Yoshua Bengio. Toward causal representation learning. *Proceedings of the IEEE*, 109(5): 612–634, 2021.

Ramprasaath R Selvaraju, Michael Cogswell, Abhishek Das, Ramakrishna Vedantam, Devi Parikh, and Dhruv Batra. Grad-cam: Visual explanations from deep networks via gradient-based localization. In *IEEE/CVF International Conference on Computer Vision*, 2017.

Harshay Shah, Kaustav Tamuly, Aditi Raghunathan, Prateek Jain, and Praneeth Netrapalli. The pitfalls of simplicity bias in neural networks. In *Advances in Neural Information Processing Systems*, 2020.

Ali Sharif Razavian, Hossein Azizpour, Josephine Sullivan, and Stefan Carlsson. Cnn features off-the-shelf: An astounding baseline for recognition. In *IEEE/CVF Conference on Computer Vision and Pattern Recognition workshops*, 2014.

Zheyan Shen, Peng Cui, Tong Zhang, and Kun Kunag. Stable learning via sample reweighting. In *AAAI Conference on Artificial Intelligence*, 2020.

Yuge Shi, Jeffrey Seely, Philip HS Torr, N Siddharth, Awni Hannun, Nicolas Usunier, and Gabriel Synnaeve. Gradient matching for domain generalization. In *International Conference on Learning Representations*, 2022.

Xiangchen Song, Weiran Yao, Yewen Fan, Xinshuai Dong, Guangyi Chen, Juan Carlos Niebles, Eric Xing, and Kun Zhang. Temporally disentangled representation learning under unknown nonstationarity. In *Advances in Neural Information Processing Systems*, 2023.

Peter Sorrenson, Carsten Rother, and Ullrich Köthe. Disentanglement by nonlinear ica with general incompressible-flow networks (gin). In *International Conference on Learning Representations*, 2020.

Charles Spearman. The proof and measurement of association between two things. *The American Journal of Psychology*, 15(1):72–101, 1904.

Jithendaraa Subramanian, Yashas Annadani, Ivaxi Sheth, Stefan Bauer, Derek Nowrouzezahrai, and Samira Ebrahimi Kahou. Latent variable models for bayesian causal discovery. In *International Conference on Machine Learning Workshop on Spurious Correlations, Invariance, and Stability*, 2022.

Hugo Touvron, Louis Martin, Kevin Stone, Peter Albert, Amjad Almahairi, Yasmine Babaei, Nikolay Bashlykov, Soumya Batra, Prajjwal Bhargava, Shruti Bhosale, et al. Llama 2: Open foundation and fine-tuned chat models. *arXiv preprint arXiv:2307.09288*, 2023.

Burak Varıcı, Emre Acartürk, Karthikeyan Shanmugam, Abhishek Kumar, and Ali Tajer. Score-based causal representation learning with interventions. In *Advances in Neural Information Processing Systems Workshop on Causal Representation Learning*, 2023.

Burak Varıcı, Emre Acartürk, Karthikeyan Shanmugam, and Ali Tajer. General identifiability and achievability for causal representation learning. In *International Conference on Artificial Intelligence and Statistics*, 2024.

Julius Von Kügelgen, Yash Sharma, Luigi Gresele, Wieland Brendel, Bernhard Schölkopf, Michel Besserve, and Francesco Locatello. Self-supervised learning with data augmentations provably isolates content from style. In *Advances in Neural Information Processing Systems*, 2021.

Julius von Kügelgen, Michel Besserve, Wendong Liang, Luigi Gresele, Armin Kekić, Elias Bareinboim, David M Blei, and Bernhard Schölkopf. Nonparametric identifiability of causal representations from unknown interventions. In *Advances in Neural Information Processing Systems*, 2023.

Lan Wang and Vishnu Naresh Boddeti. Do learned representations respect causal relationships? In *IEEE/CVF Conference on Computer Vision and Pattern Recognition*, 2022.

Yunxia Wang, Fuyuan Cao, Kui Yu, and Jiye Liang. Efficient causal structure learning from multiple interventional datasets with unknown targets. In *AAAI Conference on Artificial Intelligence*, 2022.

Xiaojiang Yang, Yi Wang, Jiacheng Sun, Xing Zhang, Shifeng Zhang, Zhenguo Li, and Junchi Yan. Nonlinear ica using volume-preserving transformations. In *International Conference on Learning Representations*, 2021.

Weiran Yao, Yuewen Sun, Alex Ho, Changyin Sun, and Kun Zhang. Learning temporally causal latent processes from general temporal data. In *International Conference on Learning Representations*, 2022.

Kui Yu, Lin Liu, and Jiuyong Li. Learning markov blankets from multiple interventional data sets. *IEEE Transactions on Neural Networks and Learning Systems*, 31(6):2005–2019, 2019.

Jiaqi Zhang, Chandler Squires, Kristjan Greenewald, Akash Srivastava, Karthikeyan Shanmugam, and Caroline Uhler. Identifiability guarantees for causal disentanglement from soft interventions. In *Advances in Neural Information Processing Systems*, 2023.

Yang Zhang, Fuli Feng, Xiangnan He, Tianxin Wei, Chonggang Song, Guohui Ling, and Yongdong Zhang. Causal intervention for leveraging popularity bias in recommendation. In *International ACM SIGIR Conference on Research and Development in Information Retrieval*, 2021.

Yujia Zheng, Ignavier Ng, and Kun Zhang. On the identifiability of nonlinear ica: Sparsity and beyond. In *Advances in Neural Information Processing Systems*, 2022.

Xiao Zhou, Yong Lin, Renjie Pi, Weizhong Zhang, Renzhe Xu, Peng Cui, and Tong Zhang. Model agnostic sample reweighting for out-of-distribution learning. In *International Conference on Machine Learning*, pp. 27203–27221. PMLR, 2022.

Roland S Zimmermann, Yash Sharma, Steffen Schneider, Matthias Bethge, and Wieland Brendel. Contrastive learning inverts the data generating process. In *International Conference on Machine Learning*, 2021.

Overview of Appendix

App. A: Details of implementation and hyperparameters for all experiments
App. B: Theoretical Motivation for RepLIn
App. C: Review of Identifiable Causal Representation Learning
App. E: Visualization of Feature Distribution Learned on WINDMILL dataset
App. D: Generating WINDMILL dataset

A Implementation details

We implement our models using PyTorch (Paszke et al., 2019) and use Adam (Kingma & Ba, 2015) as our optimizer with its default settings. Training hyperparameters for each dataset (such as the number of data points, training epochs, etc.) are shown in Tab. 5. For training stability, we warm up λ_{dep} from 0 to its set value between sN and eN epochs where N is the total number of epochs, and s and e are fractions shown in Tab. 5.

Table 5: List of hyperparameters used for each dataset.

Dataset	#Training samples	Epochs	Batchsize	Initial LR	Scheduler	λ_{dep}	λ_{self}	Start (s)	End (e)
WINDMILL	40,000	5000	1000	2e-3	MultiStepLR(milestones=[1000], gamma=0.5)	1	1	0.66	0.99
CelebA	30,000	2000	1000	1e-3	MultiStepLR(milestones=[1000], gamma=0.1)	20	2	0.01	0.99

For all methods, we first extract label-specific features from the inputs and pass them through a corresponding classifier to predict the label. The architecture of the feature extractor is the same for all methods on a given dataset, except on the WINDMILL dataset. The classification layer is a linear layer mapping from feature dimensions to the number of classes. The specific details for each dataset are provided below.

Windmill dataset: For ERM baselines, we use an MLP with two layers of size 40 and 1, with a ReLU activation after each layer (except the last) to extract the features. However, we observed that enforcing independence using 1-dimensional features was difficult. Therefore, we used 2-dimensional features for RepLIn, which were then normalized to lie on a sphere.

CelebA dataset: We first extract features from the raw image using a ResNet-50 (He et al., 2016) pretrained on ImageNet (Deng et al., 2009). Although these features are not optimal for face attribute prediction, they are useful for face verification (Sharif Razavian et al., 2014). Additionally, it makes the binary attribute prediction task more challenging. We extract attribute-specific features from this input using a linear layer that maps it to a 500-dimensional space.

B Theoretical Motivation for RepLIn

In Sec. 3.4, we theoretically motivated RepLIn. This section explains the motivation with detailed proof.

Sketch of proof: First, we estimate the statistical risk in predicting the latent variables from interventional data from representations learned by arbitrary linear feature extractors and classifiers. In this statistical risk, we will identify a term that is the source of performance drop during interventions. We will then show that the optimal ERM models will suffer from this performance drop when trained on a dataset comprising observational and interventional data. Finally, we show that minimizing linear dependence between interventional features can lead to robust linear feature extractors.

Setup: We follow the same mathematical notation as the main paper, shown in Tab. 6. The input data $\boldsymbol{X}$ is generated as a function of two latent variables of interest, A and B. There are noise variables collectively denoted by $\boldsymbol{U}$ that participate in the data generation but are not of learning interest. Our task is to predict A and B from $\boldsymbol{X}$. A and B are causally related during observation. For ease of exposition, we will consider a simple linear relation $B \coloneqq w_{AB}A$. This causal relation breaks when we intervene on B. The intervened variable is denoted with an added apostrophe (i.e., B'). The data generation process can be written in the form of a structural causal model as follows:

Entity	Notation	Examples
Scalar	Regular lowercase characters	a, γ
Random variable	Regular sans-serif uppercase characters	A
Random vector	Bold sans-serif uppercase characters	$\boldsymbol{A}$
Distribution of a random variable A	P with subscript	P_A

Table 6: Mathematical notation used in the proof.

$$\begin{array}{cc} A \sim P_A & X_A \coloneqq w_A A + U_A \\ B' \sim P_{B'} & X_B \coloneqq w_B B + U_B \\ B \coloneqq w_{AB} A \text{ (during observations)} & \\ B \coloneqq B' \text{ (during interventions)} & \boldsymbol{X} = \begin{bmatrix} X_A \\ X_B \end{bmatrix} \\ U_A, U_B \sim P_{\mathsf{U}} & \end{array}$$

Training: The distribution from which training data is sampled is denoted by P_{train}. The training data consists of both observational and interventional samples, which themselves come from distributions P_{obs} and P_{int}. We are interested in the scenario where $(1-\beta)$ proportion of the training data is observational, while the remaining β proportion is interventional, where $0 < \beta < 1$. The training distribution can be represented as a mixture of observational and interventional distributions as follows:

$$P_{\text{train}}(\boldsymbol{X}, A, B) = (1-\beta) P_{\text{obs}}(\boldsymbol{X}, A, B) + \beta P_{\text{int}}(\boldsymbol{X}, A, B)$$

Typically, we assume $\beta \ll 1$. We will also assume that A, B, $\boldsymbol{U}$, and $\boldsymbol{X}$ have zero mean, so that we may use linear models without bias terms to extract representations corresponding to the variables of interest and train linear classifiers on these representations. The corresponding classifiers are parameterized by $\boldsymbol{c}^{(\mathsf{A})}$ and $\boldsymbol{c}^{(\mathsf{B})}$. The predictions are made by the classifiers from the learned representations as $\hat{A} = \boldsymbol{c}^{(\mathsf{A})\top} \boldsymbol{\Theta}^{(A)\top} \boldsymbol{X}$ and $\hat{B} = \boldsymbol{c}^{(\mathsf{B})\top} \boldsymbol{\Theta}^{(B)\top} \boldsymbol{X}$. The models are trained by minimizing the mean squared error on the training data, $\mathcal{L}_{\text{MSE}} = \mathbb{E}_{P_{\text{train}}} \left[\left(\left\| A - \hat{A} \right\|_2^2 + \left\| B - \hat{B} \right\|_2^2 \right) \right]$.

B.1 Statistical Risk in Predicting Interventional Latent Samples

The model predicts $\hat{A}$ and $\hat{B}$ from $\boldsymbol{X}$ during inference. The statistical squared error in predicting A from interventional samples can be written as,

$$E_A = \mathbb{E}_{P_{\text{int}}} \left[\left(A - \hat{A} \right)^2 \right] = \mathbb{E}_{P_{\text{int}}} \left[\left(A - \boldsymbol{c}^{(\mathsf{A})\top} \boldsymbol{\Theta}^{(A)\top} \boldsymbol{X} \right)^2 \right] \tag{6}$$

The expectation is taken over the interventional distribution over $\boldsymbol{X}, A, B, \boldsymbol{U}$ denoted by P_{int}. $\boldsymbol{\Theta}^{(A)}$ can be written in terms of constituent parameter vectors as $\boldsymbol{\Theta}^{(A)} = \begin{bmatrix} \boldsymbol{\theta}_A^{(A)\top} \\ \boldsymbol{\theta}_B^{(A)\top} \end{bmatrix}$. The predicted latent $\hat{A}$ can hence be written in terms of these vectors as,

$$\begin{aligned} \hat{A} = \boldsymbol{c}^{(\mathsf{A})\top} \boldsymbol{\Theta}^{(A)\top} \boldsymbol{X} &= \boldsymbol{c}^{(\mathsf{A})\top} \left(X_A \boldsymbol{\theta}_A^{(A)} + X_{B'} \boldsymbol{\theta}_B^{(A)} + \boldsymbol{\Theta}^{(A)\top} \boldsymbol{U} \right) \\ &= w_A A \boldsymbol{c}^{(\mathsf{A})\top} \boldsymbol{\theta}_A^{(A)} + w_B B' \boldsymbol{c}^{(\mathsf{A})\top} \boldsymbol{\theta}_B^{(A)} + \boldsymbol{c}^{(\mathsf{A})\top} \boldsymbol{\Theta}^{(A)\top} \boldsymbol{U} \\ \therefore \left(A - \boldsymbol{c}^{(\mathsf{A})\top} \boldsymbol{\Theta}^{(A)\top} \boldsymbol{X} \right)^2 &= \left(\left(1 - w_A \boldsymbol{c}^{(\mathsf{A})\top} \boldsymbol{\theta}_A^{(A)} \right) A + w_B B' \boldsymbol{c}^{(\mathsf{A})\top} \boldsymbol{\theta}_B^{(A)} + \boldsymbol{c}^{(\mathsf{A})\top} \boldsymbol{\Theta}^{(A)\top} \boldsymbol{U} \right)^2 \\ &= \left(1 - w_A \boldsymbol{c}^{(\mathsf{A})\top} \boldsymbol{\theta}_A^{(A)} \right)^2 A^2 + \left(w_B \boldsymbol{c}^{(\mathsf{A})\top} \boldsymbol{\theta}_B^{(A)} \right)^2 B'^2 + \tilde{U}^2 \\ &\quad + 2 \left(1 - w_A \boldsymbol{c}^{(\mathsf{A})\top} \boldsymbol{\theta}_A^{(A)} \right) \left(w_B \boldsymbol{c}^{(\mathsf{A})\top} \boldsymbol{\theta}_B^{(A)} \right) A B' \\ &\quad + 2 \left(1 - w_A \boldsymbol{c}^{(\mathsf{A})\top} \boldsymbol{\theta}_A^{(A)} \right) \tilde{U} A + 2 \left(w_B \boldsymbol{c}^{(\mathsf{A})\top} \boldsymbol{\theta}_B^{(A)} \right) \tilde{U} B' \end{aligned} \tag{7}$$

$$\therefore E_A = \mathbb{E}_{P_{\text{int}}}\left[\left(1 - w_A \boldsymbol{c}^{(\mathsf{A})\top}\boldsymbol{\theta}_A^{(A)}\right)^2 A^2 + \left(w_B \boldsymbol{c}^{(\mathsf{A})\top}\boldsymbol{\theta}_B^{(A)}\right)^2 B'^2 + \tilde{U}^2\right]$$
$$+ 2\mathbb{E}_{P_{\text{int}}}\left[\left(1 - w_A \boldsymbol{c}^{(\mathsf{A})\top}\boldsymbol{\theta}_A^{(A)}\right)\left(w_B \boldsymbol{c}^{(\mathsf{A})\top}\boldsymbol{\theta}_B^{(A)}\right) AB'\right]$$
$$+ 2\mathbb{E}_{P_{\text{int}}}\left[\left(1 - w_A \boldsymbol{c}^{(\mathsf{A})\top}\boldsymbol{\theta}_A^{(A)}\right)\tilde{U}A + 2\left(w_B \boldsymbol{c}^{(\mathsf{A})\top}\boldsymbol{\theta}_B^{(A)}\right)\tilde{U}B'\right]$$

where $\tilde{U} = \boldsymbol{c}^{(\mathsf{A})\top}\boldsymbol{\Theta}^{(A)\top}\boldsymbol{U} = \boldsymbol{c}^{(\mathsf{A})\top}\boldsymbol{\theta}_A^{(A)}U_A + \boldsymbol{c}^{(\mathsf{A})\top}\boldsymbol{\theta}_B^{(A)}U_B$. $\boldsymbol{U}$ denotes exogenous variables that are independent of A and B. Due to interventions, we also have $A \perp\!\!\!\perp B$. The expectation of AB' will be zero since they are independent and have zero means marginally. Similarly, the expectation of the products of $\tilde{U}$ with A and B will be zero. Therefore,

$$E_A = \underbrace{\left(1 - w_A \boldsymbol{c}^{(\mathsf{A})\top}\boldsymbol{\theta}_A^{(A)}\right)^2 \rho_A^2 + \left(\boldsymbol{c}^{(\mathsf{A})\top}\boldsymbol{\theta}_A^{(A)}\right)^2 \rho_{\boldsymbol{U}_A}^2}_{E_A^{(1)}} + \underbrace{\left(w_B \boldsymbol{c}^{(\mathsf{A})\top}\boldsymbol{\theta}_B^{(A)}\right)^2 \rho_{B'}^2 + \left(\boldsymbol{c}^{(\mathsf{A})\top}\boldsymbol{\theta}_B^{(A)}\right)^2 \rho_{\boldsymbol{U}_B}^2}_{E_A^{(2)}} \tag{8}$$

where $\rho_A^2 = \mathbb{E}_{P_{\text{int}}}\left[A^2\right]$, $\rho_{B'}^2 = \mathbb{E}_{P_{\text{int}}}\left[B'^2\right]$, $\rho_{\boldsymbol{U}_A}^2 = \mathbb{E}_{P_{\text{int}}}\left[U_A^2\right]$, and $\rho_{\boldsymbol{U}_B}^2 = \mathbb{E}_{P_{\text{int}}}\left[U_B^2\right]$.

Statistical risk for a robust model: We are interested in robustness against interventional distribution shifts. The predictions of A by a robust model are unaffected by interventions on its child variable B. If $\hat{A}$ must not depend on B', then the corresponding representations $\boldsymbol{\phi}^{(\mathsf{A})}$ must not depend on it either, i.e. $\boldsymbol{\theta}_B^{(A)}$ must be a zero vector. Eq. (8) has two terms: $E_A^{(1)}$ and $E_A^{(2)}$. Therefore, a robust model will have $E_A^{(2)} = 0$ since $\boldsymbol{\theta}_B^{(A)} = \boldsymbol{0}$. We will show that an optimal model trained using ERM will have a non-zero $\boldsymbol{\theta}_B^{(A)}$.

B.2 Optimal ERM model

The optimal ERM model can be obtained by minimizing the expected risk in predicting the latent attributes. Since parameters are not shared between the prediction of $\boldsymbol{a}$ and $\boldsymbol{b}$, we can consider their optimization separately. We will consider the optimization of the parameters for predicting $\boldsymbol{a}$ since we are interested in the performance drop in predicting A from interventional data.

$$\boldsymbol{\Theta}^{(A)*}, \boldsymbol{c}^{(\mathsf{A})*} = \underset{\boldsymbol{\Theta}^{(A)}, \boldsymbol{c}^{(\mathsf{A})}}{\operatorname{argmin}}\ \mathbb{E}_{P_{\text{train}}}\left[\left(A - \boldsymbol{c}^{(\mathsf{A})\top}\boldsymbol{\Theta}^{(A)\top}\boldsymbol{X}\right)^2\right]$$

where P_{train} is the joint distribution of $(\boldsymbol{X}, A, B)$ during training. As mentioned earlier, P_{train} is a mixture of observational distribution P_{obs} and interventional distribution P_{int}, with $(1-\beta)$ and β acting as the mixture weights. Therefore, the training objective can be rewritten as,

$$\boldsymbol{\Theta}^{(A)*}, \boldsymbol{c}^{(\mathsf{A})*} = \underset{\boldsymbol{\Theta}^{(A)}, \boldsymbol{c}^{(\mathsf{A})}}{\operatorname{argmin}}\ J(\boldsymbol{\Theta}^{(A)}, \boldsymbol{c}^{(\mathsf{A})})$$
$$\text{where, } J(\boldsymbol{\Theta}^{(A)}, \boldsymbol{c}^{(\mathsf{A})}) = \left((1-\beta)\mathbb{E}_{P_{\text{obs}}}\left[\left(A - \boldsymbol{c}^{(\mathsf{A})\top}\boldsymbol{\Theta}^{(A)\top}\boldsymbol{X}\right)^2\right] + \beta\mathbb{E}_{P_{\text{int}}}\left[\left(A - \boldsymbol{c}^{(\mathsf{A})\top}\boldsymbol{\Theta}^{(A)\top}\boldsymbol{X}\right)^2\right]\right) \tag{9}$$

Expanding the error term on observational data, we have,

$$\boldsymbol{c}^{(\mathsf{A})\top}\boldsymbol{\Theta}^{(A)\top}\boldsymbol{X} = \boldsymbol{c}^{(\mathsf{A})\top}\left(X_A\boldsymbol{\theta}_A^{(A)} + X_B\boldsymbol{\theta}_B^{(A)} + \boldsymbol{\Theta}^{(A)\top}\boldsymbol{U}\right)$$
$$= w_A A\boldsymbol{c}^{(\mathsf{A})\top}\boldsymbol{\theta}_A^{(A)} + w_B B\boldsymbol{c}^{(\mathsf{A})\top}\boldsymbol{\theta}_B^{(A)} + \boldsymbol{c}^{(\mathsf{A})\top}\boldsymbol{\Theta}^{(A)\top}\boldsymbol{U}$$
$$= w_A A\boldsymbol{c}^{(\mathsf{A})\top}\boldsymbol{\theta}_A^{(A)} + w_B w_{AB} A\boldsymbol{c}^{(\mathsf{A})\top}\boldsymbol{\theta}_B^{(A)} + \boldsymbol{c}^{(\mathsf{A})\top}\boldsymbol{\Theta}^{(A)\top}\boldsymbol{U}$$
$$\therefore \left(A - \boldsymbol{c}^{(\mathsf{A})\top}\boldsymbol{\Theta}^{(A)\top}\boldsymbol{X}\right)^2 = \left(A - w_A A\boldsymbol{c}^{(\mathsf{A})\top}\boldsymbol{\theta}_A^{(A)} - w_B w_{AB} A\boldsymbol{c}^{(\mathsf{A})\top}\boldsymbol{\theta}_B^{(A)} - \boldsymbol{c}^{(\mathsf{A})\top}\boldsymbol{\Theta}^{(A)\top}\boldsymbol{U}\right)^2$$
$$= \left(\left(1 - w_A\boldsymbol{c}^{(\mathsf{A})\top}\boldsymbol{\theta}_A^{(A)} - w_B w_{AB}\boldsymbol{c}^{(\mathsf{A})\top}\boldsymbol{\theta}_B^{(A)}\right)A - \boldsymbol{c}^{(\mathsf{A})\top}\boldsymbol{\Theta}^{(A)\top}\boldsymbol{U}\right)^2$$
$$= \left(1 - w_A\boldsymbol{c}^{(\mathsf{A})\top}\boldsymbol{\theta}_A^{(A)} - w_B w_{AB}\boldsymbol{c}^{(\mathsf{A})\top}\boldsymbol{\theta}_B^{(A)}\right)^2 A^2 + \tilde{U}^2$$
$$- 2\left(1 - w_A\boldsymbol{c}^{(\mathsf{A})\top}\boldsymbol{\theta}_A^{(A)} - w_B w_{AB}\boldsymbol{c}^{(\mathsf{A})\top}\boldsymbol{\theta}_B^{(A)}\right)A\tilde{U}$$

where $\tilde{U} = \boldsymbol{c}^{(\mathsf{A})\top}\boldsymbol{\Theta}^{(A)\top}\boldsymbol{U} = U_A\boldsymbol{c}^{(\mathsf{A})\top}\boldsymbol{\theta}_A^{(A)} + U_B\boldsymbol{c}^{(\mathsf{A})\top}\boldsymbol{\theta}_B^{(A)}$ from App. B.1. Since the exogenous variable $\boldsymbol{U}$ is independent of A and B, the expectation of their products over the observational distribution becomes zero. Therefore,

$$\begin{aligned}\mathbb{E}_{P_{\text{obs}}}\left[\left(A - \boldsymbol{c}^{(\mathsf{A})\top}\boldsymbol{\Theta}^{(A)\top}\boldsymbol{X}\right)^2\right] &= \left(1 - w_A\boldsymbol{c}^{(\mathsf{A})\top}\boldsymbol{\theta}_A^{(A)} - w_Bw_{AB}\boldsymbol{c}^{(\mathsf{A})\top}\boldsymbol{\theta}_B^{(A)}\right)^2\mathbb{E}_{P_{\text{obs}}}\left[A^2\right] + \mathbb{E}_{P_{\text{obs}}}\left[\tilde{U}^2\right] \\ &= \left(1 - w_A\boldsymbol{c}^{(\mathsf{A})\top}\boldsymbol{\theta}_A^{(A)} - w_Bw_{AB}\boldsymbol{c}^{(\mathsf{A})\top}\boldsymbol{\theta}_B^{(A)}\right)^2\rho_A^2 + \left(\boldsymbol{c}^{(\mathsf{A})\top}\boldsymbol{\theta}_A^{(A)}\right)^2\rho_{\boldsymbol{U}_A}^2 + \left(\boldsymbol{c}^{(\mathsf{A})\top}\boldsymbol{\theta}_B^{(A)}\right)^2\rho_{\boldsymbol{U}_B}^2\end{aligned} \tag{10}$$

Note that, $\rho_A^2 = \mathbb{E}_{P_{\text{obs}}}\left[A^2\right]$, $\rho_{\boldsymbol{U}_A}^2 = \mathbb{E}_{P_{\text{obs}}}\left[U_A^2\right]$, and $\rho_{\boldsymbol{U}_B}^2 = \mathbb{E}_{P_{\text{obs}}}\left[U_B^2\right]$ similar to App. B.1 since these values are unaffected by interventions. The expansion of the error term on interventional data was derived in Eq. (8). Thus, the overall training objective Eq. (9) can be written as,

$$\begin{aligned}J(\boldsymbol{\Theta}^{(A)}, \boldsymbol{c}^{(\mathsf{A})}) = (1-\beta)&\left(\left(1 - w_A\boldsymbol{c}^{(\mathsf{A})\top}\boldsymbol{\theta}_A^{(A)} - w_Bw_{AB}\boldsymbol{c}^{(\mathsf{A})\top}\boldsymbol{\theta}_B^{(A)}\right)^2\rho_A^2 + \left(\boldsymbol{c}^{(\mathsf{A})\top}\boldsymbol{\theta}_A^{(A)}\right)^2\rho_{\boldsymbol{U}_A}^2 + \left(\boldsymbol{c}^{(\mathsf{A})\top}\boldsymbol{\theta}_B^{(A)}\right)^2\rho_{\boldsymbol{U}_B}^2\right) \\ &+ \beta\left(\left(1 - w_A\boldsymbol{c}^{(\mathsf{A})\top}\boldsymbol{\theta}_A^{(A)}\right)^2\rho_A^2 + \left(w_B\boldsymbol{c}^{(\mathsf{A})\top}\boldsymbol{\theta}_B^{(A)}\right)^2\rho_{B'}^2 + \left(\boldsymbol{c}^{(\mathsf{A})\top}\boldsymbol{\theta}_A^{(A)}\right)^2\rho_{\boldsymbol{U}_A}^2 + \left(\boldsymbol{c}^{(\mathsf{A})\top}\boldsymbol{\theta}_B^{(A)}\right)^2\rho_{\boldsymbol{U}_B}^2\right)\end{aligned}$$

We set $\psi_1 = \boldsymbol{c}^{(\mathsf{A})\top}\boldsymbol{\theta}_A^{(A)}$ and $\psi_2 = \boldsymbol{c}^{(\mathsf{A})\top}\boldsymbol{\theta}_B^{(A)}$. Since ERM jointly optimizes the feature extractors and the classifiers, no unique solution minimizes the prediction loss. For example, scaling the feature extractor parameters by an arbitrary constant scalar γ and the classifier parameters by $1/\gamma$ will give the same error. Therefore, we can optimize $J(\boldsymbol{\Theta}^{(A)}, \boldsymbol{c}^{(\mathsf{A})})$ over ψ_1 and ψ_2, similar to (Arjovsky et al., 2019).

$$\begin{aligned}J(\boldsymbol{\Theta}^{(A)}, \boldsymbol{c}^{(\mathsf{A})}) = (1-\beta)&\left(\left(1 - w_A\psi_1 - w_Bw_{AB}\psi_2\right)^2\rho_A^2 + \psi_1^2\rho_{\boldsymbol{U}_A}^2 + \psi_2^2\rho_{\boldsymbol{U}_B}^2\right) \\ &+ \beta\left(\left(1 - w_A\psi_1\right)^2\rho_A^2 + w_B^2\psi_2^2\rho_{B'}^2 + \psi_1^2\rho_{\boldsymbol{U}_A}^2 + \psi_2^2\rho_{\boldsymbol{U}_B}^2\right)\end{aligned} \tag{11}$$

The optimal values of ψ_1 and ψ_2 are the stationary points of $J(\boldsymbol{\Theta}^{(A)}, \boldsymbol{c}^{(\mathsf{A})})$ (denoted by J for brevity). Thus the optimal parameter values can be solved for by taking the first-order derivatives of J w.r.t. ψ_1 and ψ_2 and setting them to zero.

$$\begin{aligned}\frac{\partial J}{\partial \psi_1} &= 2(1-\beta)\left(-\left(1 - w_A\psi_1 - w_Bw_{AB}\psi_2\right)w_A\rho_A^2 + \psi_1\rho_{\boldsymbol{U}_A}^2\right) + 2\beta\left(-\left(1 - w_A\psi_1\right)w_A\rho_A^2 + \psi_1\rho_{\boldsymbol{U}_A}^2\right) \\ \frac{\partial J}{\partial \psi_2} &= 2(1-\beta)\left(-\left(1 - w_A\psi_1 - w_Bw_{AB}\psi_2\right)w_Bw_{AB}\rho_A^2 + \psi_2\rho_{\boldsymbol{U}_B}^2\right) + 2\beta\left(w_B^2\psi_2\rho_{B'}^2 + \psi_2\rho_{\boldsymbol{U}_B}^2\right)\end{aligned}$$

Setting $\frac{\partial J}{\partial \psi_1} = \frac{\partial J}{\partial \psi_2} = 0$, we have,

$$\begin{aligned}\left(w_A^2\rho_A^2 + \rho_{\boldsymbol{U}_A}^2\right)\psi_1 &+(1-\beta)w_Aw_Bw_{AB}\rho_A^2\psi_2 &-w_A\rho_A^2 &= 0 \\ (1-\beta)w_Aw_Bw_{AB}\rho_A^2\psi_1 &+\left(\beta w_B^2\rho_{B'}^2 + (1-\beta)w_B^2w_{AB}^2\rho_A^2 + \rho_{\boldsymbol{U}_B}^2\right)\psi_2 &-(1-\beta)w_Bw_{AB}\rho_A^2 &= 0\end{aligned}$$

The equations are of the form $u_1\psi_1 + v_1\psi_2 + w_1 = 0$ and $u_2\psi_1 + v_2\psi_2 + w_2 = 0$. We can solve for ψ_2 as $\psi_2 = \frac{w_2u_1 - w_1u_2}{v_1u_2 - v_2u_1}$. Since we are only interested in probing the robustness of ERM models, we will check if ψ_2 is zero instead of fully solving the system of linear equations. $E_{\mathsf{A}}^{(2)}$ in Eq. (8) is zero if $\psi_2 = 0$, i.e. if $w_2u_1 - w_1u_2 = 0$.

$$\begin{aligned}w_2u_1 - w_1u_2 &= -(1-\beta)w_Bw_{AB}\left(w_A^2\rho_A^2 + \rho_{\boldsymbol{U}_A}^2\right)\rho_A^2 + 4(1-\beta)w_A^2w_Bw_{AB}\rho_A^4 \\ &= -(1-\beta)w_Bw_{AB}\rho_A^2\rho_{\boldsymbol{U}_A}^2\end{aligned}$$

Unless the training data is entirely composed of interventional data (i.e., $\beta = 1$), $w_2u_1 - w_1u_2$ is not zero. Thus, the optimal ERM model is not robust against interventional distribution shifts.

B.3 Minimizing Linear Dependence

In Sec. 3.3, we showed that dependence between interventional features correlated positively with the drop in accuracy on interventional data. We will now verify if minimizing dependence between interventional features can minimize the drop in accuracy. For ease of exposition, we will minimize the linear dependence between interventional features instead of enforcing statistical independence. The interventional features are given by $\boldsymbol{F}_A = \boldsymbol{\Theta}^{(A)\top}\boldsymbol{X}$ and $\boldsymbol{F}'_B = \boldsymbol{\Theta}^{(B)\top}\boldsymbol{X}$.

$$\begin{aligned}
\boldsymbol{F}_A = \boldsymbol{\Theta}^{(A)\top}\boldsymbol{X} &= \begin{bmatrix}\boldsymbol{\theta}_A^{(A)} & \boldsymbol{\theta}_B^{(A)}\end{bmatrix}\begin{bmatrix}X_A \\ X_B\end{bmatrix} \\
&= X_A\boldsymbol{\theta}_A^{(A)} + X_B\boldsymbol{\theta}_B^{(A)} \\
\boldsymbol{F}'_B = \boldsymbol{\Theta}^{(B)\top}\boldsymbol{X} &= \begin{bmatrix}\boldsymbol{\theta}_A^{(B)} & \boldsymbol{\theta}_B^{(B)}\end{bmatrix}\begin{bmatrix}X_A \\ X_B\end{bmatrix} \\
&= X_A\boldsymbol{\theta}_A^{(B)} + X_B\boldsymbol{\theta}_B^{(B)}
\end{aligned}$$

To define linear independence between interventional features, we use the following definition of cross-covariance from (Gretton et al., 2005):

Definition 1. *The* cross-covariance operator *associated with the joint probability p_{XY} is a linear operator $C_{XY} : \mathcal{G} \to \mathcal{F}$ defined as*

$$C_{XY} = \mathbb{E}_{XY}\left[(\phi(X) - \mu_X) \otimes (\psi(Y) - \mu_Y)\right]$$

where $\mathcal{G}$ and $\mathcal{F}$ are reproducing kernel Hilbert spaces (RKHSs) defined by feature maps ϕ and ψ respectively, and $\otimes$ is the tensor product defined as follows

$$(f \otimes g)h \coloneqq f\langle g, h\rangle_{\mathcal{G}} \text{ for all } h \in \mathcal{G}$$

where $\langle\cdot,\cdot\rangle$ is the inner product defined over $\mathcal{G}$.

In our case, instead of RKHS, we have finite-dimensional feature space $\mathbb{R}^d$. Therefore, we have the cross-covariance matrix as follows,

$$C_{XY} = \mathbb{E}_{XY}\left[\phi(X) \otimes \psi(Y)\right] = \mathbb{E}_{XY}\left[\phi(X)\psi(Y)^\top\right]$$

given that the feature maps have zero mean. Following the definition of HSIC (Gretton et al., 2005), linear dependence in the finite-dimensional case between X and Y is defined as the Frobenius norm of the cross-covariance matrix. Therefore, we define the linear dependence loss between the interventional features as,

$$\mathcal{L}_{\text{dep}} = \text{Dep}\left(\boldsymbol{F}_A, \boldsymbol{F}'_B\right) = \left\|\mathbb{E}_{P_{\text{int}}}\left[\boldsymbol{F}_A\boldsymbol{F}_B'^\top\right]\right\|_F^2 \tag{12}$$

Leveraging the independence relations during interventions, we can expand Eq. (12) as,

$$\begin{aligned}
\mathbb{E}_{P_{\text{int}}}\left[\boldsymbol{F}_A\boldsymbol{F}_B'^\top\right] &= \mathbb{E}_{P_{\text{int}}}\left[\left(X_A\boldsymbol{\theta}_A^{(A)} + X_B\boldsymbol{\theta}_B^{(A)}\right)\left(X_A\boldsymbol{\theta}_A^{(B)} + X_B\boldsymbol{\theta}_B^{(B)}\right)^\top\right] \\
&= \mathbb{E}_{P_{\text{int}}}\left[X_A^2\boldsymbol{\theta}_A^{(A)}\boldsymbol{\theta}_A^{(B)\top} + X_AX_B\boldsymbol{\theta}_A^{(A)}\boldsymbol{\theta}_B^{(B)\top} + X_AX_B\boldsymbol{\theta}_B^{(A)}\boldsymbol{\theta}_A^{(B)\top} + X_B^2\boldsymbol{\theta}_B^{(A)}\boldsymbol{\theta}_B^{(B)\top}\right] \\
&= (w_A^2\rho_A^2 + \rho_{\boldsymbol{U}_A}^2)\boldsymbol{\theta}_A^{(A)}\boldsymbol{\theta}_A^{(B)\top} + (w_B^2\rho_{B'}^2 + \rho_{\boldsymbol{U}_B}^2)\boldsymbol{\theta}_B^{(A)}\boldsymbol{\theta}_B^{(B)\top} \\
\therefore \mathcal{L}_{\text{dep}} &= \left\|(w_A^2\rho_A^2 + \rho_{\boldsymbol{U}_A}^2)\boldsymbol{\theta}_A^{(A)}\boldsymbol{\theta}_A^{(B)\top} + (w_B^2\rho_{B'}^2 + \rho_{\boldsymbol{U}_B}^2)\boldsymbol{\theta}_B^{(A)}\boldsymbol{\theta}_B^{(B)\top}\right\|_F^2
\end{aligned}$$

In the last step, all cross-covariance terms are zero due to the independence of the corresponding random variables in the causal graph. The dependence loss is the Frobenius norm of a sum of rank-one matrices $\boldsymbol{\theta}_A^{(A)}\boldsymbol{\theta}_A^{(B)\top}$ and $\boldsymbol{\theta}_B^{(A)}\boldsymbol{\theta}_B^{(B)\top}$. Consider the following general form: $\boldsymbol{Z} = \boldsymbol{a}\boldsymbol{b}^\top + \boldsymbol{c}\boldsymbol{d}^\top$. Then $Z_{ij} = a_ib_j + c_id_j$.

$$\|\boldsymbol{Z}\|_F^2 = \sum_{ij}\left(a_ib_j + c_id_j\right)^2$$

$\|\boldsymbol{Z}\|_F^2$ is a sum of squares and thus is zero iff $a_i b_j + c_i d_j = 0$, $\forall i, j$. Therefore, $\mathcal{L}_{\text{dep}}$ is minimized when $\theta_{Ai}^{(A)}\theta_{Aj}^{(B)} + \theta_{Bi}^{(A)}\theta_{Bj}^{(B)} = 0$, $\forall i, j$. The potential solutions that minimize $\mathcal{L}_{\text{dep}}$ are (1) $\boldsymbol{\theta}_A^{(A)} = \boldsymbol{\theta}_B^{(A)} = \boldsymbol{\theta}_A^{(B)} = \boldsymbol{\theta}_B^{(B)} = \mathbf{0}$, (2) $\boldsymbol{\theta}_A^{(A)} = \pm\gamma\boldsymbol{\theta}_B^{(A)}$ and $\gamma\boldsymbol{\theta}_A^{(B)} = \mp\boldsymbol{\theta}_B^{(B)}$ for some $\gamma \neq 0$, and (3) $\boldsymbol{\theta}_A^{(A)} = \mathbf{0}$ or $\boldsymbol{\theta}_A^{(B)} = \mathbf{0}$, and $\boldsymbol{\theta}_B^{(A)} = \mathbf{0}$ or $\boldsymbol{\theta}_B^{(B)} = \mathbf{0}$. The former two solutions result in trivial features and will increase the classification error. The latter solution contains four possible solutions, out of which two solutions result in trivial features. Solutions resulting in trivial features are unlikely to occur during optimization due to a large classification error. Therefore, we need to consider only the remaining two solutions.

The possible solutions are: (1) $\boldsymbol{\theta}_A^{(A)} = \mathbf{0}, \boldsymbol{\theta}_B^{(B)} = \mathbf{0}$, and (2) $\boldsymbol{\theta}_B^{(A)} = \mathbf{0}, \boldsymbol{\theta}_A^{(B)} = \mathbf{0}$. Intuitively, in the former solution, A and B will be predicted using X_B and X_A respectively, and the latter solution corresponds to a robust feature extractor that minimizes the reducible error in Eq. (8). We will compare the predictive error achieved by these solutions to compare their likelihood during training.

Recall the expression for training error in predicting A from Eq. (11).

$$\begin{aligned}
J_A(\boldsymbol{\Theta}^{(A)}, \boldsymbol{c}^{(\mathsf{A})}) &= (1-\beta)\left(\left(1 - w_A\psi_{A1} - w_B w_{AB}\psi_{A2}\right)^2 \rho_A^2 + \psi_{A1}^2\rho_{\boldsymbol{U}_A}^2 + \psi_{A2}^2\rho_{\boldsymbol{U}_B}^2\right) \\
&\quad + \beta\left(\left(1 - w_A\psi_{A1}\right)^2 \rho_A^2 + w_B^2\psi_{A2}^2\rho_{B'}^2 + \psi_{A1}^2\rho_{\boldsymbol{U}_A}^2 + \psi_{A2}^2\rho_{\boldsymbol{U}_B}^2\right) \\
&= (1-\beta)\left(\left(1 - w_A\psi_{A1} - w_B w_{AB}\psi_{A2}\right)^2 \rho_A^2\right) \\
&\quad + \beta\left(\left(1 - w_A\psi_{A1}\right)^2 \rho_A^2 + w_B^2\psi_{A2}^2\rho_{B'}^2\right) + \psi_{A1}^2\rho_{\boldsymbol{U}_A}^2 + \psi_{A2}^2\rho_{\boldsymbol{U}_B}^2
\end{aligned}$$

We use ψ_{A1} and ψ_{A2} instead of ψ_1 and ψ_2 respectively to denote the parameters for predicting A. A similar expression can be written for the error in predicting B with ψ_{B1} and ψ_{B2} denoting the parameters for predicting B.

$$\begin{aligned}
J_B(\boldsymbol{\Theta}^{(B)}, \boldsymbol{c}^{(\mathsf{B})}) &= (1-\beta)\left(\left(1 - w_A\psi_{B1} - w_B w_{AB}\psi_{B2}\right)^2 \rho_A^2 + \psi_{B1}^2\rho_{\boldsymbol{U}_A}^2 + \psi_{B2}^2\rho_{\boldsymbol{U}_B}^2\right) \\
&\quad + \beta\left(w_A^2\psi_{B1}^2\rho_A^2 + (1 - w_B\psi_{B2})^2\rho_{B'}^2 + \psi_{B1}^2\rho_{\boldsymbol{U}_A}^2 + \psi_{B2}^2\rho_{\boldsymbol{U}_B}^2\right) \\
&= (1-\beta)\left(\left(1 - w_A\psi_{B1} - w_B w_{AB}\psi_{B2}\right)^2 \rho_A^2\right) \\
&\quad + \beta\left(w_A^2\psi_{B1}^2\rho_A^2 + (1 - w_B\psi_{B2})^2\rho_{B'}^2\right) + \psi_{B1}^2\rho_{\boldsymbol{U}_A}^2 + \psi_{B2}^2\rho_{\boldsymbol{U}_B}^2
\end{aligned}$$

Case 1: When $\boldsymbol{\theta}_A^{(A)} = \mathbf{0}, \boldsymbol{\theta}_B^{(B)} = \mathbf{0}$: In this case, $\psi_{A1} = 0$ and $\psi_{B2} = 0$. Therefore, the predictive error during training for each latent variable can be written as,

$$\begin{aligned}
J_A &= (1-\beta)\left(w_B w_{AB}\psi_{A2} - 1\right)^2 \rho_A^2 + \beta\rho_A^2 + \beta w_B^2\psi_{A2}^2\rho_{B'}^2 + \psi_{A2}^2\rho_{\boldsymbol{U}_B}^2 \\
J_B &= (1-\beta)\left(w_A\psi_{B1} - w_{AB}\right)^2 \rho_A^2 + \beta w_A^2\psi_{B1}^2\rho_A^2 + \beta\rho_{B'}^2 + \psi_{B1}^2\rho_{\boldsymbol{U}_A}^2
\end{aligned}$$

The optimal values of ψ_{A2} and ψ_{B1} can be obtained by equating the gradients of R_A and R_B to zero.

$$\begin{aligned}
\frac{\partial J_A}{\partial \psi_{A2}} &= 2(1-\beta) w_B w_{AB}\left(w_B w_{AB}\psi_{A2} - 1\right)\rho_A^2 + 2\beta w_B^2\psi_{A2}\rho_{B'}^2 + 2\psi_{A2}\rho_{\boldsymbol{U}_B}^2 = 0 \\
\therefore \psi_{A2}^* &= \frac{(1-\beta) w_B w_{AB}\rho_A^2}{(1-\beta) w_B^2 w_{AB}^2\rho_A^2 + \beta w_B^2\rho_{B'}^2 + \rho_{\boldsymbol{U}_B}^2} \\
J_A^* &= \frac{(1-\beta)\rho_A^2\left(\beta w_B^2\rho_{B'}^2 + \rho_{\boldsymbol{U}_B}^2\right)}{(1-\beta) w_B^2 w_{AB}^2\rho_A^2 + \beta w_B^2\rho_{B'}^2 + \rho_{\boldsymbol{U}_B}^2} + \beta\rho_A^2
\end{aligned}$$

$$\begin{aligned}
\frac{\partial J_B}{\partial \psi_{B1}} &= 2(1-\beta) w_A\left(w_A\psi_{B1} - w_{AB}\right)\rho_A^2 + 2\beta w_A^2\psi_{B1}\rho_A^2 + 2\psi_{B1}\rho_{\boldsymbol{U}_A}^2 = 0 \\
\therefore \psi_{B1}^* &= \frac{(1-\beta) w_A w_{AB}\rho_A^2}{w_A^2\rho_A^2 + \rho_{\boldsymbol{U}_A}^2} \\
J_B^* &= \frac{(1-\beta) w_{AB}^2\rho_A^2(\beta w_A^2\rho_A^2 + \rho_{\boldsymbol{U}_A}^2)}{w_A^2\rho_A^2 + \rho_{\boldsymbol{U}_A}^2} + \beta\rho_{B'}^2
\end{aligned}$$

The combined training error for this solution is,

$$\begin{aligned} J_1^* &= J_A^* + J_B^* \\ &= \frac{(1-\beta)\rho_A^2\left(\beta w_B^2\rho_{B'}^2 + \rho_{\boldsymbol{U}_B}^2\right)}{(1-\beta)w_B^2w_{AB}^2\rho_A^2 + \beta w_B^2\rho_{B'}^2 + \rho_{\boldsymbol{U}_B}^2} + \beta\rho_A^2 \\ &\quad + \frac{(1-\beta)w_{AB}^2\rho_A^2(\beta w_A^2\rho_A^2 + \rho_{\boldsymbol{U}_A}^2)}{w_A^2\rho_A^2 + \rho_{\boldsymbol{U}_A}^2} + \beta\rho_{B'}^2 \end{aligned} \tag{13}$$

Case 2: When $\boldsymbol{\theta}_B^{(A)} = \mathbf{0}, \boldsymbol{\theta}_A^{(B)} = \mathbf{0}$: Here, $\psi_{A2} = 0$ and $\psi_{B1} = 0$. The predictive error during training for each latent variable can be written as,

$$\begin{aligned} J_A &= \left(w_A\psi_{A1} - 1\right)^2\rho_A^2 + \psi_{A1}^2\rho_{\boldsymbol{U}_A}^2 \\ J_B &= \left((1-\beta)w_{AB}^2\rho_A^2 + \beta\rho_{B'}^2\right)\left(w_B\psi_{B2} - 1\right)^2 + \psi_{B2}^2\rho_{\boldsymbol{U}_B}^2 \end{aligned}$$

We follow the former procedure to estimate the optimal values of ψ_{A1} and ψ_{B2}.

$$\begin{aligned} \frac{\partial J_A}{\partial \psi_{A1}} &= 2w_A\left(w_A\psi_{A1} - 1\right)\rho_A^2 + 2\psi_{A1}\rho_{\boldsymbol{U}_A}^2 = 0 \\ \therefore \psi_{A1}^* &= \frac{w_A\rho_A^2}{w_A^2\rho_A^2 + \rho_{\boldsymbol{U}_A}^2} \\ J_A^* &= \frac{\rho_A^2\rho_{\boldsymbol{U}_A}^2}{w_A^2\rho_A^2 + \rho_{\boldsymbol{U}_A}^2} \end{aligned}$$

$$\begin{aligned} \frac{\partial J_B}{\partial \psi_{B2}} &= 2w_B\left((1-\beta)w_{AB}^2\rho_A^2 + \beta\rho_{B'}^2\right)\left(w_B\psi_{B2} - 1\right) + 2\psi_{B2}\rho_{\boldsymbol{U}_B}^2 \\ \therefore \psi_{B2}^* &= \frac{(1-\beta)w_Bw_{AB}^2\rho_A^2 + \beta w_B\rho_{B'}^2}{(1-\beta)w_B^2w_{AB}^2\rho_A^2 + \beta w_B^2\rho_{B'}^2 + \rho_{\boldsymbol{U}_B}^2} \\ J_B^* &= \frac{\left((1-\beta)w_{AB}^2\rho_A^2 + \beta\rho_{B'}^2\right)\rho_{\boldsymbol{U}_B}^2}{(1-\beta)w_B^2w_{AB}^2\rho_A^2 + \beta w_B^2\rho_{B'}^2 + \rho_{\boldsymbol{U}_B}^2} \end{aligned}$$

The combined training error for this solution is,

$$\begin{aligned} J_2^* &= J_A^* + J_B^* \\ &= \frac{\rho_A^2\rho_{\boldsymbol{U}_A}^2}{w_A^2\rho_A^2 + \rho_{\boldsymbol{U}_A}^2} + \frac{\left((1-\beta)w_{AB}^2\rho_A^2 + \beta\rho_{B'}^2\right)\rho_{\boldsymbol{U}_B}^2}{(1-\beta)w_B^2w_{AB}^2\rho_A^2 + \beta w_B^2\rho_{B'}^2 + \rho_{\boldsymbol{U}_B}^2} \end{aligned} \tag{14}$$

Comparing J_1^* and J_2^*,

$$\begin{aligned} J_1^* - J_2^* = &\frac{(1-\beta)\beta w_B^2\rho_A^2\rho_{B'}^2 + (1-\beta)\rho_A^2\rho_{\boldsymbol{U}_B}^2 - (1-\beta)w_{AB}^2\rho_A^2\rho_{\boldsymbol{U}_B}^2 - \beta\rho_{B'}^2\rho_{\boldsymbol{U}_B}^2}{(1-\beta)w_B^2w_{AB}^2\rho_A^2 + \beta w_B^2\rho_{B'}^2 + \rho_{\boldsymbol{U}_B}^2} \\ &+ \frac{(1-\beta)\beta w_A^2w_{AB}^2\rho_A^4 + (1-\beta)w_{AB}^2\rho_A^2\rho_{\boldsymbol{U}_A}^2 - \rho_A^2\rho_{\boldsymbol{U}_A}^2}{w_A^2\rho_A^2 + \rho_{\boldsymbol{U}_A}^2} + \beta(\rho_A^2 + \rho_{B'}^2) \end{aligned}$$

Simplifying the above expression, we get the condition that $J_1^* - J_2^* > 0$ if β satisfies the following conditions: (1) $\beta \geq 1 - \frac{1}{|w_{AB}|}$, (2) $\beta \geq \min\left(\frac{\rho_A^2}{2\rho_{B'}^2 + \rho_A^2}, \frac{\rho_{\boldsymbol{U}_A}^2}{w_A^2w_{AB}^2\rho_A^2}\right)$. The conditions imply that enforcing linear independence results in robust feature extractors when *enough* interventional data is available during training.

However, this is only a sufficient condition that strictly ensures $J_1^* - J_2^* > 0$. In practice, β could be much lower, especially when the total loss is of the form $\mathcal{L}_{\text{total}} = \lambda_{\text{MSE}}\mathcal{L}_{\text{MSE}} + \lambda_{\text{dep}}\mathcal{L}_{\text{dep}}$, where λ_{MSE} and λ_{dep}

are positive hyperparameters. We verify this empirically by randomly setting the parameters of the data generation process and plotting the predictive errors J_1^* and J_2^* for different values of β. We calculate J_1^* and J_2^* for 5000 runs (shown using thin curves) and plot the average error (shown using thick curves) in Fig. 12. We observe that the average value of J_1^* is always higher than that of J_2^* for all values of β. But, when $\beta \to 0$, their average values get closer to each other.

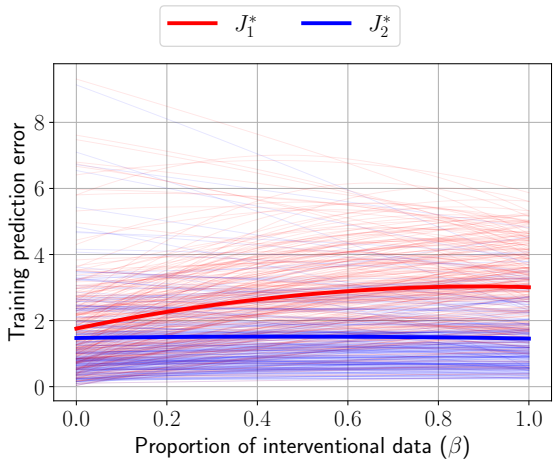

Figure 12: Comparing J_1^* (Eq. (13)) and J_2^* (Eq. (14)) as functions of β for 5000 runs with randomly sampled data generation parameters. We show individual runs using thin curves and the average error values using thick curves. We only show the errors from a few randomly sampled runs for visual clarity. We observe that the average value of J_1^* (shown using thick red curve) is always higher than that of J_2^* (shown using thick blue curve), indicating that enforcing linear independence between interventional features is more likely to obtain robust feature extractors than degenerate solutions.

C Review of identifiable causal representation learning

The primary objective of identifiable causal representation learning (ICRL) is to learn a representation such that it is possible to identify the latent factors (up to permutation and elementwise transformation) from the representation. These methods are commonly built upon autoencoder-based approaches and learn generative representations. The advantage of learning a causal representation is that the decoder then implicitly acts as the true underlying causal model, facilitating counterfactual evaluation and interpretable representations.

Locatello et al. (2019); Khemakhem et al. (2020) showed that disentangled representation learning was impossible without additional assumptions on both the model and the data. Some of the inductive biases that have been proposed since to learn disentangled representations include auxiliary labels (Hyvarinen & Morioka, 2016; Hyvarinen et al., 2019; Sorrenson et al., 2020; Khemakhem et al., 2020; Lu et al., 2021; Ahuja et al., 2022b; Kong et al., 2022), temporal data (Klindt et al., 2021; Yao et al., 2022; Song et al., 2023), and assumptions on the mixing function (Sorrenson et al., 2020; Yang et al., 2021; Lachapelle et al., 2022; Zheng et al., 2022; Moran et al., 2022).

Use of interventional data: Some works also use interventional data as weak supervision for identifiable representation learning (Lippe et al., 2022b; Brehmer et al., 2022; Ahuja et al., 2022a; 2023; Varıcı et al., 2023; von Kügelgen et al., 2023). Lippe et al. (2022b) learns identifiable representations from temporal sequences with possible interventions at any time step. Similar to our setting, they assume the knowledge of the intervention target. They also assume that the intervention on a latent variable at a time step does not affect other latent variables in the same time step. Lippe et al. (2023) relaxes the latter assumption as long as perfect interventions with known targets are available. Von Kügelgen et al. (2021); Zimmermann et al. (2021) showed that self-supervised learning with data augmentations allowed for identifiable representation learning. Brehmer et al. (2022) use pairs of data samples before and after some unknown intervention to learn latent causal models. Ahuja et al. (2022a) learns identifiable representations from sparse perturbations,

with identifiability guarantees depending on the sparsity of these perturbations. Sparse perturbations can be treated as a parent class of interventions where the latent is intervened through an external action such as in reinforcement learning. Ahuja et al. (2022b) use interventional data for causal learning for polynomial mixing functions, under some assumptions on the nature of support for non-intervened variables. Varıcı et al. (2024) relaxes the polynomial assumption on the mixing function and proves identifiability when two uncoupled hard interventions per node are available along with observational data. Varıcı et al. (2023) learn identifiable representations from data observed under different interventional distributions with the help of the score function during interventions. von Kügelgen et al. (2023) uses interventional data to learn identifiable representations up to nonlinear scaling. In addition to the above uses of interventional data, a few works (Saengkyongam & Silva, 2020; Saengkyongam et al., 2024; Zhang et al., 2023) have also attempted to predict the effect of unseen joint interventions with the help of observational and atomic interventions under various assumptions on the underlying causal model.

Difference from our setting: The general objective in ICRL is to "learn both the true joint distribution over both observed and latent variables" (Khemakhem et al., 2020). In contrast, the objective of our work is to learn representations corresponding to latent variables that are robust against interventional distributional shifts by leveraging *known* interventional independence relations. We pursue this objective in the hope that as large models such as (Radford et al., 2021), (Brown et al., 2020), (Touvron et al., 2023) and (Dehghani et al., 2023) become more ubiquitous, efficient methods to improve these models with minimal amounts of experimentally collected data will be of interest.

D Generating Windmill Dataset

We provide the exact mathematical formulation of Windmill dataset described in Sec. 3.1. We define the following constants:

Constants	Description	Default value
n_{arms}	Number of "arms" in Windmill dataset	4
$r_{\max}$	Radius of the circular region spanned by the observed data	2
θ_{wid}	Angular width of each arm	$\frac{0.9\pi}{n_{\text{arms}}} = 0.7068$
λ_{off}	Offset wavelength. Determines the complexity of the dataset	6
$\theta_{\text{max-off}}$	Maximum offset for the angle	$\pi/6$

Table 7: Constants used for generating Windmill dataset, their meaning, and their values.

$$
\begin{aligned}
R_B &\sim \mathcal{B}(1, 2.5) && \text{(Sample radius)}\\
R &= \frac{r_{\max}}{2}\left(BR_B + (1-B)(2-R_B)\right) && \text{(Modify sampled radius based on } B\text{)}\\
\Theta_A &\sim \mathcal{C}\left(\left\{2\pi\frac{i}{n_{\text{arms}}+1} : i = 0, \ldots, n_{\text{arms}}-1\right\}\right) && \text{(Choose an arm)}\\
U &\sim \mathcal{U}(0,1) && \text{(To choose a random angle)}\\
\Theta_{\text{off}} &= \theta_{\text{max-off}} \sin\left(\pi\lambda_{\text{off}}\frac{R}{r_{\max}}\right) && \text{(Calculate radial offset for the angle)}\\
\Theta &= \theta_{\text{wid}}\,(U-0.5) + A\left(\Theta_A + \frac{\pi}{n_{\text{arms}}}\right) + (1-A)\Theta_A + \Theta_{\text{off}}\\
& && \text{(Angle is decided by } A \text{ and the radial offset)}\\
X_1 = R\cos\Theta, X_2 &= R\sin\Theta, X = \begin{bmatrix} X_1 \\ X_2 \end{bmatrix} && \text{(Convert to Cartesian coordinates)}
\end{aligned}
$$

PyTorch code to generate Windmill dataset is provided in Listing 1.

Listing 1: Code for WINDMILL dataset

```
import math
import torch

# Constants
num_arms = 4 # number of blades in the windmill
max_th_offset = 0.5236 # max offset that can be added to the angle for shearing (= pi/6)
r_max = 2 # length of the blade
num_p = 20000 # number of points to be generated
offset_wavelength = 6 # adjusts the complexity of the blade

# Sample latent variables according to the causal graph.
A = torch.bernoulli(torch.ones(num_points) * 0.6)
if observational_data:
    B = A
else:
    B = torch.bernoulli(torch.ones(num_points) * 0.5)

# Convert A, B to X.
th_A0 = torch.linspace(0, 2*math.pi, num_arms+1)[:-1]
th_A1 = torch.linspace(0, 2*math.pi, num_arms+1)[:-1] + math.pi/num_arms
# Choose a random arm for A=0 from possible arms. Likewise for A=1.
th_A0 = th_A0[torch.randint(num_arms, (num_p,))]
th_A1 = th_A1[torch.randint(num_arms, (num_p,))]

# beta distribution with alpha=1, beta=3
beta_dist = torch.distributions.beta.Beta(1, 2.5)

# Sample r according to B. If B=0, sample a small r, else sample a large r.
# r ranges from 0 to r_max
B0_r = beta_dist.sample(torch.Size([num_p])) * r_max/2.
B1_r = r_max - beta_dist.sample(torch.Size([num_p])) * r_max/2.
r = B * B0_r + (1-B) * B1_r

# Sample theta according to A.
# Choose the theta arm according to A and then sample from this arm using a uniform distribution.

# First we will have a cartwheel style.
theta = torch.rand(num_p)*th_wid + th_A0*(1-A) + th_A1*A - th_wid/2.

# Add an offset to theta according to r.
th_offset_mod = torch.sin((r/r_max)*offset_wavelength*math.pi)
th_offset = max_th_offset*th_offset_mod
theta += th_offset

x1 = r*torch.cos(theta)
x2 = r*torch.sin(theta)

data = torch.stack([x1, x2], dim=1)
labels = torch.stack([A, B], dim=1).type(torch.long)
```

E Visualization of Feature Distribution Learned on Windmill dataset

In this section, we compare the feature distributions learned by RepLIn on WINDMILL dataset against all the baselines from Sec. 5.1. The feature distributions are shown in Fig. 13.

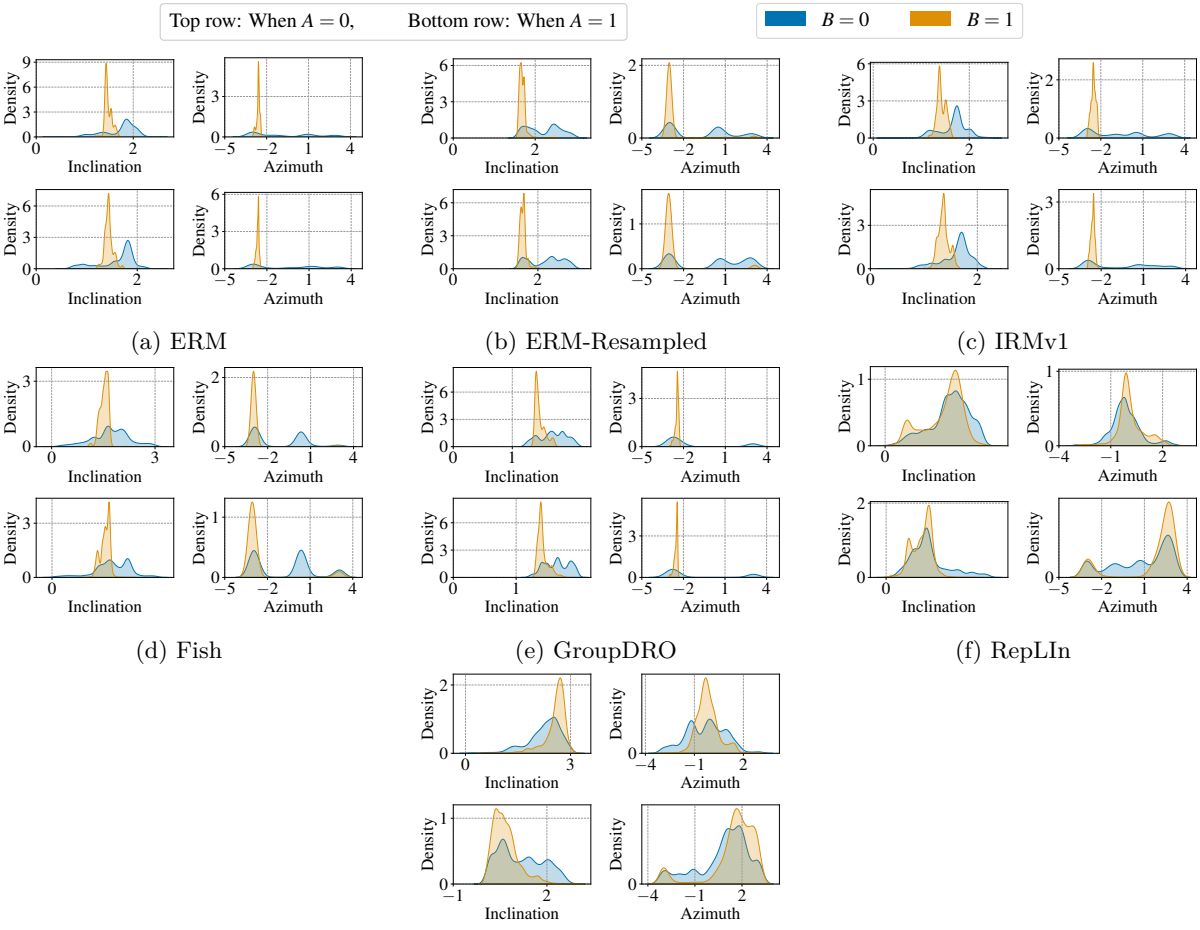

(a) ERM (b) ERM-Resampled (c) IRMv1

(d) Fish (e) GroupDRO (f) RepLIn

(g) RepLIn-Resampled

Figure 13: Visualization of interventional features learned by various methods on WINDMILL dataset.